Geometry and shape inversion in Choanoeca flexa

Figs/University_Crest.pdf

Adam Konkol

Advisor: Dr. R. E. Gold-
stein

Department of Physics
University of Cambridge

This thesis is submitted for the degree of
Master of Philosophy

Churchill College   July 2022

I would like to dedicate this thesis to my loving parents . . .

ak2351: dedicate to people!

Declaration

I hereby declare that except where specific reference is made to the work of others, the contents of this dissertation are original and have not been submitted in whole or in part for consideration for any other degree or qualification in this, or any other university. This thesis is my own work and includes nothing which is the outcome of work done in collaboration except where specifically indicated in the text. This thesis contains fewer than 15,000 words including appendices, bibliography, footnotes, and tables.

Adam Konkol
July 2022

Acknowledgements

And I would like to acknowledge ...

> ak2351: acknowledge people!

Abstract

The newly discovered multicellular choanoflagellate Choanoeca flexa forms a curved sheet that undergoes a functional, light-triggered inversion. This change in orientation that allows the organism to reversibly switch between efficient swimming and feeding shapes provides an opportunity to study biological exploitation of geometry in an evolutionarily basal context. I sought to model the mechanics that produce this apparent bistability and the dynamics of the active transformation between the two states.

In this work, I approach the modeling problem from complementary continuous and discrete mechanics perspectives. Since radial expansion and contraction at a given latitude require azimuthal stretching and shrinking, a one-dimensional filament model does not capture the energetic barriers encountered by the sheet during the transition. Using energy functional variation, I solve for the forces acting throughout the sheet and derive corresponding equilibrium shape equations. Both views establish that C. flexa inversion can be hindered in sufficiently large sheets by cell collars connecting adjacent cells stretching.

Comparisons between the discrete model for C. flexa mechanics and previously published experimental results support that collar stretching at the edges interferes in sheet inversion. Treating the organism as a crystal lattice defined by cells and cell-cell interactions, we recognise that the graph degree of cells plays a substantial role in overall sheet curvature and ability to invert.

My results suggest that the graph topology of the cell-cell interface network must accommodate inversion, particularly at the edge of the sheet. Future work should image C. flexa flipping and observe changes in connectivity that accompany the transition. My results link graph topology with a notion of surface curvature through established ideas in the theory of crystal structure.

Table of contents

List of figures

List of tables

Nomenclature

boundary cells cells with free collar microvilli

Chapter 1

Introduction

1.1   Background

Thesis statement: studying evolutionarily basal organisms lets us study the simple ways that nature exploits geometry in living systems without higher order functional complications.

Discuss evolutionary origins of multicellularity and some basic examples like Volvox. What drives organisms to become multicellular?

The organisms in the *Volvox* genus are well studied for being a primitive example of multicellularity and a shining beacon of functional geometric changes. These organisms attach their cells to one another using an extra-cellular matrix, as *S. rosetta* does as well (discussed later).

We are interested in multicellularity at an evolutionarilty basal level to understand the basic reasons that life evolved to form multicellular organisms. Sponges are as basal as multicellular animal life goes

ak2351: Discuss why and reference a review about sponges evolutionary simplicity. Carr et al. [5] could be a good ref to give here regarding choanoflagellates

.

While we are interested in sponges since they are members of the animal kingdom, choanoflagellates are often considered to be evolutionarily and morphologically comparable.

1.2   Choanoflagellates

ak2351: Discuss Carr et al. [5] about molecular phylogeny of choanoflagellates

Mah et al. [16] offers the first comprehensive comparison between sponge choanocyte and choanoflagellate morphology. Sponge collars are fairly cylindrical while choanoflagellate collars are more cone-like. Choanoflagellates have glycocalyx, but seemingly around the cell body [15]. Notably the collars in choanoflagellates are always microvillar and always present, while in sponges they emerge as a consequence of cell differentiation

> ak2351: cite this!

.

> ak2351: this is an old connection, though. James-Clark (1868) first describes the similarities. Tuzet (1963) finds that tehy have a common ancestor but not that sponges evolved from choanoflagellates. see references in first paragraph of Leadbeater [14].

Choanoflagellates are increasingly studied as a model for understanding how multicellular animal life emerged. Fairclough et al. [8] shows that the transition from single cell to multicellular colony in *Salpingoeca rosetta* occurs by cell division, with cells remaining attached to each other.

S. rosetta has an extracellular matrix [11]. Larson et al. [11] finds that the extracellular matrix constrains cells to grow and divide to a given colony shape. This paper also finds that *S. rosetta* does not have distinct cell lineages or a developmental plan.

Kirkegaard and Goldstein [9] finds that collared choanoflagellates drive the most flow through their collars by swimming fastest, which occurs in the unicellular state [17]. This makes it unclear that forming rosette colonies is for the sake of improved feeding. The authors point to evidence that *S. rosetta* is induced to form rosette colonies by bacterial cues to suggest that the reasons for the development of multicellularity may be more subtle than previously expected [1].

1.3 *Choanoeca flexa*

Brunet et al. [3] describe a newly discovered choanoflagellate, *Choanoeca flexa*, which lives and feeds in aquatic environments. Here, I describe the relevant properties and characteristics of these cells and their colonies for modeling its structure and behavior. All descriptions proceed from Brunet et al. [3] and private communications with the authors.

Another sheet forming-choanoflagellate was described in Leadbeater [14], *Proterospongia choanojuncta*. The literature is full of other choanoflagellates also forming colonies with curved geometries, i.e. Lauterborn [12].

Nor is *C. flexa* the first choanoflagellate observed to have a contractile process that influences collar angle. The only other member of *Choanoeca*, *C. perplexa*, has also been

observed to feature a rapid, dramatic adduction/abduction of the collar microvilli between 10° and 90° from the apicobasal axis [7]. Leadbeater [13] described contractions at the base of the collars that occur with changes in the collar angle. Remaining wary of the risk of speculating for *C. flexa*, Leadbeater [13] speculated that colonies of *C. perplexa* form by daughter cells remaining attached after division. This is supported by the observed mechanism of individual cell division, where daughter cells are temporarily connected at a late stage by some collar microvilli.

Shape inversion: swimming/feeding, light triggered, dynamics of process Connected by collars, (presumed) active transformation via contractile ring. This differs from choanoflagellates like *S. rosetta* which use ECM [11]. Likely stiff actin collars with some intrinsic curvature and potentially different stiffness between the two states.

If other choanoflagellates are any indication, we know in *S. rosetta* that cell division is asynchronous [8]. If *C. flexa* forms colonies by a similar mechanism, then we might not expect regularity in its structure.

> ak2351: this need not be true! What would asynchronous cell division indicate about structure?

We are interested in this species because we hope we can use its colonies' geometries as a model for sponge choanocyte chambers and more broadly to understand how life most simply exploits shape at a multicellular level. It is quite difficult to experimentally model flows in the choanocyte chamber [?], and published results on choanocyte flow have only been computational. Understanding the geometry of *C. flexa* can contribute to understanding the flows that a colony can drive, which will contribute to the growing body of knowledge on flows driven by several pumps positioned along a surface [2].

1.4   Thesis overview

The thesis will be structured in this way.

Chapter 2

Continuous model

Sheets of *C. flexa*, despite being discretely made up of individual cells, appear to take on curvature when looked at as a whole. In an effort to develop an analytically tractable model for sheets consisting of many cells and avoid buildilng a detailed network topology, I approximate here sheets of *C. flexa* using continuous functions.

I begin by developing a one-dimensional filament model with inversion dynamics, which demonstrates that azimuthal stretching is key to understanding the flipping process observed in Brunet et al. [3]. I proceed to describe a method for approximating sheets of *C. flexa* with two-dimensional surfaces and relate the collar-opening angle ϕ and collar-collar contact angle ψ to surface curvature. I write an expression for the sheet energy and vary it to derive a shape equation.

2.1   One-dimensional model

ak2351: Discuss when a continuous model is appropriate

We are interested in the problem of *Choaneca flexa* inversion. To build intuition, consider a chain of cells connected by their collar filaments like beads on a string. Supposing there are sufficiently many cells that the length contributed to the chain of cells by a single cell is small relative to the total length, we approximate the filament with a continuous function $\vec{r}(s)$ parameterised by arclength s. If the filament has preferred curvature κ_0, then the bending energy functional ε is given by

$$\varepsilon[\vec{r}(s)] = \frac{1}{2}A \int (\kappa - \kappa_0)^2 ds,$$

where the curvature κ is deduced from $\vec{r}(s)$ and A is the bending modulus.

If the filament is short relative to the characteristic bending length scale, we express the problem in the Mange representation by writing $\vec{r}(s) = (x, h(x))$ for a height function $h(x)$. The resulting energy is written in terms of the prescribed (signed) curvature H_0,

$$\varepsilon[\vec{h}(x)] = \frac{1}{2}A \int_0^L (h_{xx} - H_0)^2 dx. \tag{2.1}$$

Since the cells in this beads-on-a-chain description consist of large spheres connected by thin filaments, we postulate that the filament experiences isotropic drag with coefficient ζ in a viscous medium. As a result, we describe the dynamics with a functional derivative of the energy with respect to the changing height,

$$\zeta \vec{r}_t = -\frac{\delta \varepsilon}{\delta \vec{r}}$$

$$\zeta h_t = -\frac{\delta \varepsilon}{\delta h}. \tag{2.2}$$

Taking the functional derivative of equation 2.1, we find the energy change

$$\delta \varepsilon = A(h_{xx} - H_0)\delta h_x \big|_0^L - Ah_{3x}\delta h \big|_0^L + A \int h_{4x}\delta h \, ds \tag{2.3}$$

in terms of the boundary conditions of h.

For free boundary conditions (force- and torque-free edges) $h_{xx}(0,L) = 0 = h_{3x}(0,L)$, the boundary terms in equation 2.3 vanish and we are left with the equation of motion

$$\zeta h_t = -Ah_{4x}. \tag{2.4}$$

Equation 2.4 is nondimensionalised by re-expressing x as x/L and t as $t/(\frac{\zeta L^4}{A})$ (the labels x, t, h, H_0 are left unchanged for readability) to derive $h_t = -h_{4x}$ with boundary conditions $h_{xx}(0,1) = 0 = h_{3x}(0,L)$. It is clear that the ground state of equation 2.1 is given by a quadratic height function with quadratic term $\frac{1}{2}H_0 x^2$. Let $h_*(x) = -\frac{1}{2}H_0(x - \frac{1}{2})^2 + \frac{1}{8}H_0$ be one such ground state, and suppose $h(x,0) = -h_*(x)$. Note that the filament in $h(x,0)$ is not in the ground state since the curvature is given by H_0.

The dynamics of the displacement $g(x,t) = h(x,t) - h_*(x)$ is given by $g_t = g_{4x}$. If $g(x,t) = e^{-\sigma t} f(x)$ for some $f(x)$ and eigenvalue σ, we obtain the ordinary boundary value problem

$$\frac{d^4 f}{dx^4} = \sigma f \qquad \begin{cases} f''(0,1) = 0 \\ f'''(0,1) = 0. \end{cases} \qquad (2.5)$$

It is clear that the general solution of f is $A \sin kx + B \cos kx + D \sinh kx + E \cosh kx$ [10]. As in Wiggins et al. [20], the derivatives $f''(0) = f'''(0) = 0$ give $A = D, B = E$. Moreover, the eigenvalues $\sigma = k^4$ are given by the sequence of solutions k_n to

$$\cos k - \frac{1}{\cosh k} = 0. \qquad (2.6)$$

Equation 2.6 is plotted in Figure 2.1a along with the positions of the solutions k_n as solved numerically. The solution $k_0 = 0$ is omitted because it contributes a constant term to $h(x,t)$ that does not evolve in time. The eigenfunctions $w_n(x)$ with eigenvalues k_n^4 are normalized on the interval $[0,1]$ numerically, and the ratio A/B is given by $(\sinh k - \sin(k))/(\cosh k - \cos k)$. The first five eigenfunctions are shown in Figure 2.1b.

Chapter2/Figs/eq_roots.png

Chapter2/Figs/efuncs.png
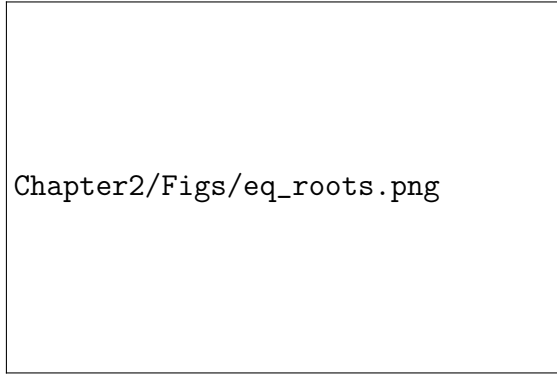
(a) Equation 2.6 and its solutions.
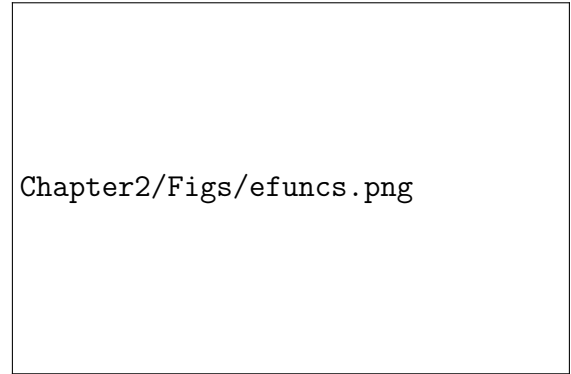
(b) The first five eigenfunctions f_n of boundary value problem 2.5.

Fig. 2.1 Solving the boundary value problem in equation 2.5

Letting $f(x) = \sum_{n=1}^{\infty} a_n f_n(x)$, we get that $a_n = \int_0^1 g(x,0) f_n(x) dx$, and the complete dynamics of the height function are given by

$$h(x,t) = h_*(x) + g(x) = h_*(x) + \sum_{n=1}^{\infty} a_n e^{k_n^4 t} f_n(x). \qquad (2.7)$$

In practice, only the solutions k_n to equation 2.6 shown in Figure 2.1a are used, since the approximation to $h(x,0)$ is close and higher k_n result in precision errors when calculating $\cosh kx$ and $\sinh kx$.

For the initial conditions given previously, the time evolution of $h(x,t)$ is shown in Figure 2.2. Immediately, we notice that the filament changes shape extremely quickly, and the timescale $\zeta L^4/A$ must be extremely large to produce inversion at the order of $10\,\text{sec}$ as observed by Brunet et al. [3]. Using Stokes' law $\zeta = 6\pi\mu R$ for dynamic viscosity μ (about $1\,\text{kg/m/sec}$) [19] and cell radius $R \approx 1 \times 10^{-6}\,\text{m}$ [3], a chain of 100 cells each contributing $5 \times 10^{-6}\,\text{m}$ length would require energy constant about

> ak2351: finish the above. compare to bending modulus of flagella or microtubule or somethin

Besides the issue of timescale, the dynamics in figure 2.2 also fail to capture the *rolling over* phenomenon observed at the edges of large sheets [3], where a wave of changing curvature propagates from the edge of the sheet towards the centre. While the edges show a slight rim around $t \approx 9 \times 10^{-4}$, the effect is not as pronounced as in *C. flexa* inversion and does not occur at the initation of the transition. A possible explanation for this effect in the cell sheets is that the collars resist compression or stretching. The representation used here, on the other hand, does not penalise filament compression.

As the arclength decreases substantially during the transition in figure 2.2 without affecting its dynamics, it is clear that collar extension and compression are essential to describing appropriate dynamics. Moreover, the timescales between this one-dimensional model and those observed experimentally being as misaligned as they are indicates that some energetic barrier to inversion is missing in the above description. We identify here the key deficiency of the one-dimensional description of *C. flexa* sheets, which is that compression and extension, especially in the azimuthal direction, are essential to understand the sheets' bistable nature.

2.2 Surface approximation

The simplified dynamics that we get from the Mange representation lack energetic costs from the compression and extension that come with deforming a two dimensional surface. The logical step to include these energies is to model the flexa sheet a surface of revolution based on a curve $\boldsymbol{r}(\rho,\theta) = (\rho\cos\theta, \rho\sin\theta, z(\rho))$ with cylindrical coordinates ρ,θ and height function z. In doing so, we could take the elastohydrodynamic equation of motion written in terms of curvature H and K and express it as purely as a function of z.

We will proceed by writing the equations of motion generally for a surface and reducing it to a surface of revolution.
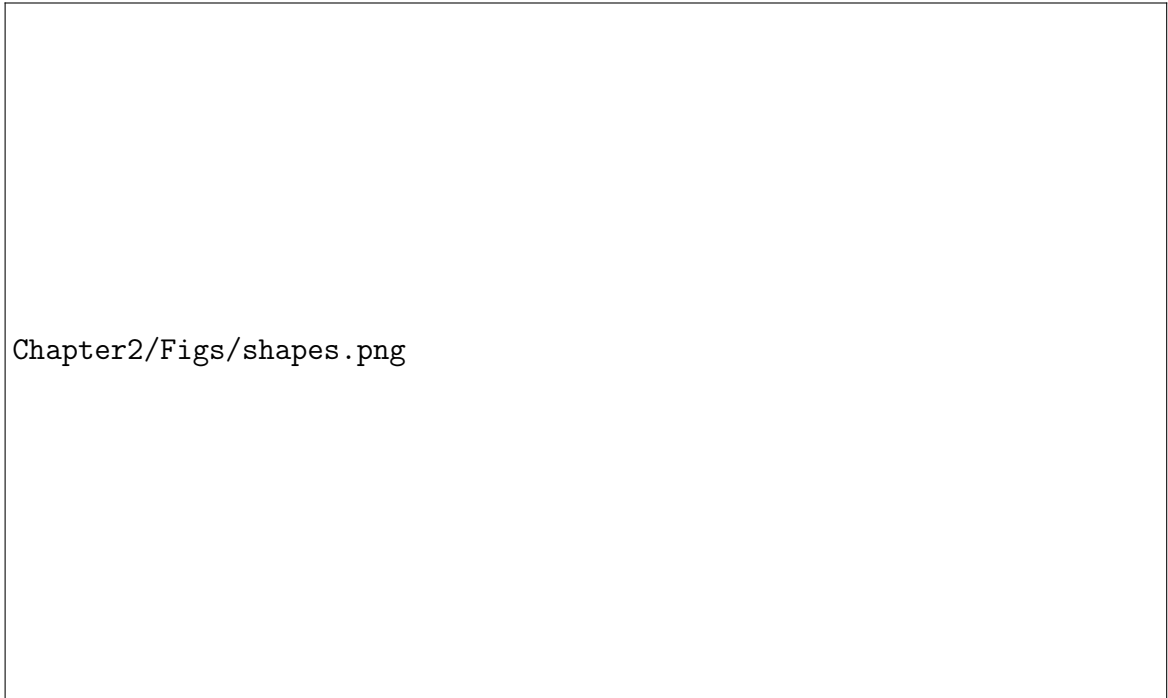
Fig. 2.2 Time evolution of a one-dimensional filament which switches prescribed curvature sign instantaneously. Time and length are given in dimensionless units defined by the length L, bending modulus A, and drag coefficient ζ. The time unlabeled time intervals continue sequentially in intervals of $\Delta t = 3 \times 10^{-4}$.

2.2.1 H and collar connection angle

Before getting into the continuous sheet problem, it is worth describing the two degrees of freedom that our collar connections afford. The collar makes an angle ϕ between the vector pointing directly out of the cell and the vector between the cell and its collar boundary with the next cell. Additionally, there is an angle between the collars of two adjacent cells ψ. The latter results in the sheet's curvature, so we want to relate it to mean curvature H or preferred curvature H_0.

> ak2351: Discuss why we need a collar angle ψ despite Brunet et al. [3] and other sources just talking about ϕ. This has to do with the straight-collar approximation that I use, where the collar shape and curvature + clamped boundary condition of the meeting collars is distilled into two angles

Fig. 2.3 Geometry for relating collar boundary angle ψ to curvature H.

      Consider two neighboring cells with collar boundaries a, b, and c, as shown in Figure 2.3. We might imagine defining a radius of curvature by the circle that passes through the three collar boundaries. If we set $\boldsymbol{x_a} = 2\ell \sin\phi_0(-1,0)$, $\boldsymbol{x_b} = (0,0)$, and $\boldsymbol{x_c} = 2\ell \sin\phi_0(\sin(\psi_0 - \phi_0), \cos(\psi_0 - \phi_0))$, we can solve for the circle coordinates

$$(x_\circ, y_\circ) = \ell \sin \phi_0 \left(-1, \frac{1 + \cos 2(\psi_0 - \phi_0)}{\sin 2(\psi_0 - \phi_0)} \right)$$

to get the inverse radius of curvature

$$H_0 = \frac{1}{\sqrt{x_\circ^2 + y_\circ^2}} = \frac{\sin(\psi_0 - \phi_0)}{\ell \sin \phi_0}. \tag{2.8}$$

This has a nice, simple interpretation in that if $\psi_0 > \phi_0$, $H_0 > 0$ (as drawn in Figure 2.3). On the other hand, $\psi_0 < \phi_0$ implies $H_0 < 0$, or the sheet is concave on the cell body side. Alternatively, we solve for ψ_0 as a function of H_0,

$$\psi_0 = \phi_0 + \arcsin\left(H_0 \ell \sin \phi_0\right). \tag{2.9}$$

As we find later in equation 2.14, the curvature of the sheet in any given direction is greater than or equal to $-1/\ell$ (cell bodies and collars cannot go through each other). This lower bound corresponds in 2.9 to $\psi_0 = 0$, which we expect when cells are pressing tightly against each other (Figure 2.5).

2.2.2   Problem statement

Powers [18] (Section IV.B) shows that for an energy density $\mathscr{E}$ written in terms of the first and second fundamental forms $g_{\alpha\beta}$ and $K_{\alpha\beta}$, we can write an expression for the stress tensor $\boldsymbol{F}^\alpha$

$$\boldsymbol{F}^\alpha = \left(T^{\alpha\beta} + \mathscr{E}^{\alpha\beta} K_\gamma^\beta\right) \boldsymbol{t}_\beta - (\nabla_\beta \mathscr{E}^{\alpha\beta}) \hat{\boldsymbol{n}}. \tag{2.10}$$

Here, $K_\gamma^\beta = K_{\gamma\delta} g^{\delta\beta}$, $\boldsymbol{t}_\beta = \partial_\beta \boldsymbol{r}$, and

$$T^{\alpha\beta} = g^{\alpha\beta} \mathscr{E} + 2\frac{\partial \mathscr{E}}{\partial g_{\alpha\beta}} = \frac{2}{\sqrt{g}} \frac{\partial}{\partial g_{\alpha\beta}} \left(\sqrt{g} \mathscr{E}\right)$$

$$\mathscr{E}^{\alpha\beta} = \frac{\partial \mathscr{E}}{\partial K_{\alpha\beta}}$$

1 with $g = \det g_{\alpha\beta}$.

2   Since the force $\boldsymbol{f}$ acting on a surface point is given by the covariant divergence of the

3 stress $\nabla_\alpha \boldsymbol{F}^\alpha$, our problem is effectively solved once we decide on an appropriate energy

4 density. Brunet et al. [3] showed that the angle formed by the *C. flexa* collars changes when

5 individual cells are triggered for inversion. We might reasonably suggest preferred sheet

6 curvature is prescribed by changing the preferred angle of the collar ϕ_0 and imposing and

7 energetic cost based on the amount that the collar angle $\phi(\theta)$ differs around the collar in θ:

8 $\mathcal{E} \sim \int (\phi(\theta) - \phi_0)^2 d\theta$.

9 ### 2.2.3   Connecting continuous surface with individual cell mechanics

10 For any point on a smooth surface, we could find an orthonormal basis of eigenvectors $\boldsymbol{e}_1, \boldsymbol{e}_2$

11 in the tangent space that diagonalises K_μ^ν. In terms of a vector $\boldsymbol{\Delta\xi}$ written in this basis, we

12 have that the change in height with respect to the tangent plane and its normal Δh is given by

13 $K_{\mu\nu} \Delta\xi^\mu \Delta\xi^\nu$.

14   Let's consider a cell with collar angle $\phi(\theta)$, where θ measures the location on the collar.

15 If the cell has an optimal collar angle ϕ_0 and corresponding optimal curvature $K_{0\mu\nu}$, then the

16 height of the collar will be $K_{0\mu\nu} \Delta\xi_0^\mu \Delta\xi_0^\nu$. The distance from the centerline of the cell (the

17 norm of $\boldsymbol{\Delta\xi_0}$) is determined by ϕ_0. The geometry is shown in Figure 2.4.

18   If the cell has collar angle ϕ in direction θ, we know the collar distance as $\boldsymbol{\Delta\xi} =$

19 $\ell(\cos\phi, \sin\phi)$. For a fixed collar length ℓ, we know the difference in height between the

20 ground state and deformed state is $\ell(\cos\phi - \cos\phi_0)$. We can then relate the collar angle and

21 sheet curvature by equating

22
23 $$K_{\mu\nu} \Delta\xi^\mu \Delta\xi^\nu - K_{0\mu\nu} \Delta\xi_0^\mu \Delta\xi_0^\nu = \ell(\cos\phi - \cos\phi_0). \tag{2.11}$$

24   The radius out from the center for the ground state is $\ell\sin\phi_0$ while for the deformed state

25 it is $\ell\sin\phi$, so for $K_{011} = K_{022} = H_0$, we get

26 $$K_{\mu\nu} \ell^2 \sin^2\phi (\cos\theta, \sin\theta)^{\mu,\nu} - H_0 \ell^2 \sin^2\phi_0 = \ell(\cos\phi - \cos\phi_0)$$

27
28 $$H_\theta \ell^2 \sin^2\phi - H_0 \ell^2 \sin^2\phi_0 = \ell(\cos\phi - \cos\phi_0)$$

29 where $H_\theta = K_{11}\cos^2\theta + K_{22}\sin^2\theta + 2K_{12}\sin\theta\cos\theta$ is the curvature of a line on the surface

30 in direction θ. We can cancel a factor of ℓ, redefine units of length in terms of ℓ (such that
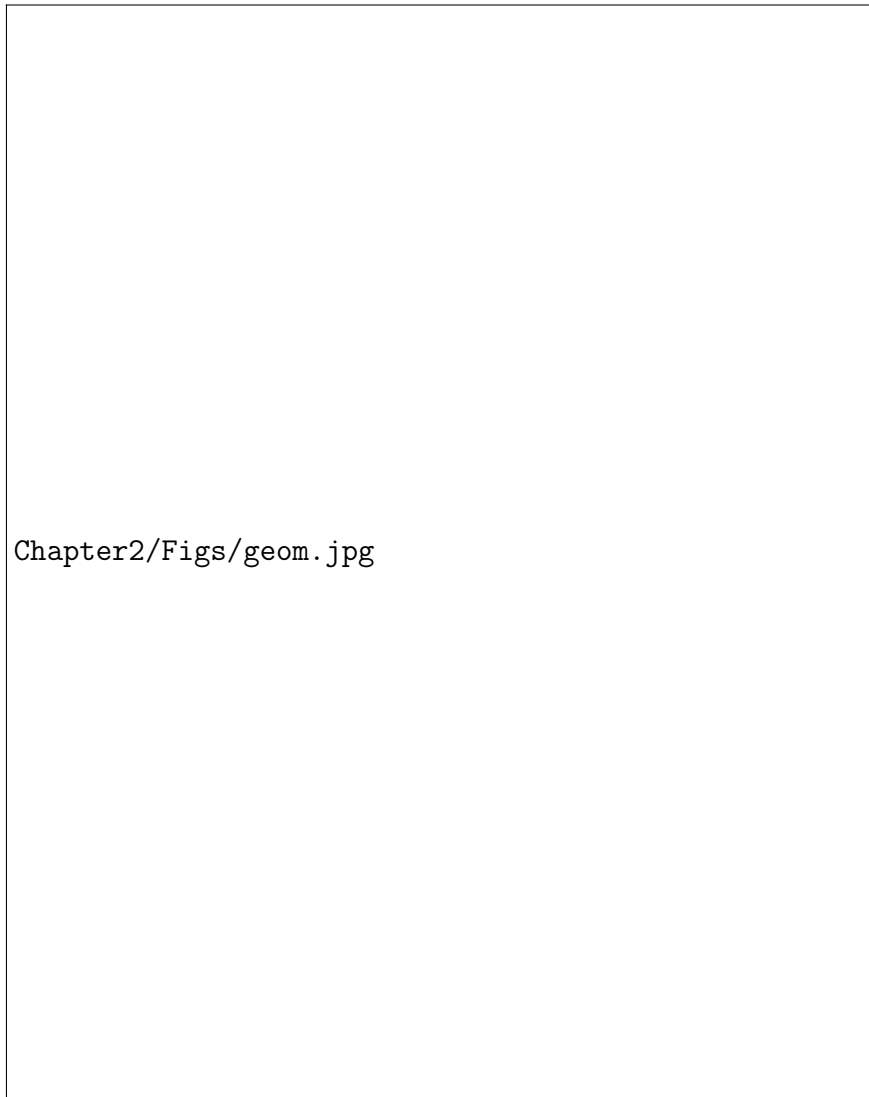
Fig. 2.4 Geometry of a single cell and collar with a continuous surface approximating the interactions between collars.

H_θ is the ratio of ℓ with the radius of curvature in direction θ), and express $\sin^2 \phi$ in terms of $\cos \phi$ to get

$$0 = H_\theta \cos^2 \phi + \cos \phi + (H_0 \sin^2 \phi_0 - \cos \phi_0 - H_\theta)$$

$$\cos \phi = \frac{-1 \pm \sqrt{1 + 4H_\theta (H_\theta + \cos \phi_0 - H_0 \sin^2 \phi_0)}}{2H_\theta}.$$

If we take the collars to always have angle $0 \leq \phi \leq \pi/2$, we can constrain $0 \leq \cos \phi \leq 1$ to find the two inequalities

$$H_\theta \geq H_0 \sin^2 \phi_0 - \cos \phi_0 \tag{2.12}$$

$$1 \geq \cos \phi_0 - H_0 \sin^2 \phi_0. \tag{2.13}$$

The second inequality can be simplified to $H_0 \geq -(1 + \cos \phi_0)^{-1}$. Combining the two inequalities yields

$$H_\theta \geq -1. \tag{2.14}$$

Re-expressed with units, this means that $H_\theta \geq -1/\ell$, or that the radius of curvature can never be smaller than ℓ on the cells' side. In other words, the cells can't push through each other! (Figure 2.5)

Fig. 2.5 Maximum cell-side curvature is given by inequalities 2.12, 2.13 to have radius ℓ. This corresponds to every (point) cell bumping into each other.

2.2.4   Writing the energy

We want to write equation 2.11 in terms of $\phi - \phi_0$ to write down the energy. We can use a trigonometric identity to write

$$H_\theta \sin^2 \phi - H_0 \sin^2 \phi_0 = -2 \sin \frac{\phi - \phi_0}{2} \sin \frac{\phi + \phi_0}{2}. \tag{2.15}$$

If $phi - phi_0$ is small in magnitude, then

$$\sin \frac{\phi - \phi_0}{2} \approx \frac{\phi - \phi_0}{2}$$

$$\sin \frac{\phi + \phi_0}{2} = \sin \left(\phi_0 + \frac{\phi + \phi_0}{2} \right) \approx \sin \phi_0 + \frac{\phi - \phi_0}{2} \cos \phi_0$$

$$\sin^2 \phi = \sin^2 (\phi_0 + (\phi - \phi_0)) \approx \sin^2 \phi_0 + (\phi - \phi_0) \sin 2\phi_0.$$

Using these approximations we rewrite equation 2.15 to first order in $\phi - \phi_0$ as

$$(H_\theta - H_0) \sin^2 \phi_0 + H_\theta (\phi - \phi_0) \sin 2\phi_0 = -(\phi - \phi_0) \sin \phi_0$$

$$(H_\theta - H_0) \sin^2 \phi_0 = -(\phi - \phi_0)(H_\theta \sin 2\phi_0 + \sin \phi_0)$$

$$\frac{(H_\theta - H_0)^2 \sin^4 \phi_0}{(H_\theta + \sin \phi_0 / \sin 2\phi_0)^2 \sin^2 2\phi_0} = (\phi - \phi_0)^2.$$

We want to integrate this function in θ, so let $K_{11} = a$, $K_{22} = b$, $K_{12} = c$, $-H_0 = d$ and $\sin \phi_0 / \sin 2\phi_0 = e$ for simplicity when we write

$$\int_{-\pi}^{\pi} (\phi - \phi_0)^2 d\theta = \int_{-\pi}^{\pi} \frac{\left(a\cos^2\theta + b\sin^2\theta + 2c\sin\theta\cos\theta + d\right)^2}{\left(a\cos^2\theta + b\sin^2\theta + 2c\sin\theta\cos\theta + e\right)^2} d\theta$$

$$= \{ -\sin 2\theta \left[a^2(-4bc\theta - 4ce\theta + d^2 - 2de + e^2) + a(4b^2c\theta - 2b(d-e)^2 + 4c\theta(c^2 - e^2)) \right.$$

$$+ b^2(4ce\theta + d^2 - 2de + e^2) + 4bc\theta(e^2 - c^2) + 4c^2(d-e)^2]$$

$$+ 2(a+b+2e)\left[c^2\theta(b-a) + \theta(a-b)(a+e)(b+e) - c(d-e)^2 \right]$$

$$+ 2\theta(a-b)^2\cos(2\theta)(a(b+e) + e(b+e) - c^2) \}$$

$$/2\left[(a-b)(a(b+e) + e(b+e) - c^2)((a-b)\cos(2\theta) + a + b + 2c\sin(2\theta) + 2e) \right]$$

$$+ \frac{(e-d)(a(4b+d+3e) + bd + 3be - 4c^2 + 2de + 2e^2)\tan^{-1}\left(\frac{-(b+e)\tan\theta - c}{\sqrt{a(b+e) + e(b+e) - c^2}} \right)}{2(a(b+e) + e(b+e) - c^2)^{3/2}}$$

evaluated at $\theta = -\pi, \pi$. Evaluating this expression is surprisingly straightforward, and gives the result

$$\int_{-\pi}^{\pi} (\phi - \phi_0)^2 d\theta = \text{const.} + \text{const.} \frac{4K + 2(d+3e)H + 2de + e^2}{(K + 2H + e^2)^{3/2}}.$$

Varying this expression will be more difficult than the typical membrane energy defined only in terms of curvature $(H - H_0)^2 + K$ since the Gaussian curvature term is not alone. This means that we cannot use the Gauss Bonnet theorem $\int_S K dA = 2\pi n + \oint_{\partial S} K ds$ to simply write it as a boundary term. Nevertheless, provided that we can vary K on the surface, the shape equation that results shouldn't be very difficult to derive.

2.2.5   Varying the energy

Following subsection 2.2.2, we just need to express our energy in terms of $K_{\mu\nu}$ and $g_{\mu\nu}$ to derive a force from it. We of course have that $H = (1/2)(K_{\mu\nu}g^{\mu\nu})$, which is easily differentiated with respect to $K_{\mu\nu}$ and $g_{\mu\nu}$. We can differentiate K by re-expressing it with the identity $K^{\alpha\beta}K_{\alpha\beta} = 4H^2 - 2K$.[1] Then we have $K = (g^{\alpha\beta}K_{\alpha\beta})^2 - K_{\mu\nu}K_{\alpha\beta}g^{\mu\alpha}g^{\nu\beta}$.

---

[1]This comes from $4H^2 - 2K = (K_1^1 + K_2^2)^2 - 2(K_1^1 K_2^2 - 2K_2^1) = (K_1^1)^2 + 2K_2^1 K_2^1 + (K_2^2)^2 = K_\beta^\alpha K_\alpha^\beta = K^{\alpha\beta}K_{\alpha\beta}$.

2.3   Energy variation

1

Chapter 3

Discrete model

Models of organisms and population dynamics must be designed by either describing potentially many discrete units[1] with continuous functions or dealing with the analytical complexity of discretisation. Even with the continuous description of *C. flexa* described previously, numerical solutions to the shape equations would require discretisation of a surface. Here, I pursue a simplified, discrete description of *C. flexa* sheets. As in chapter 2, I proceed by formulating an energy function based on the coordinate vectors of cells and vary it with respect to the coordinates. This procedure results in expressions for the forces on the coordinates, which can be forward integrated in time to study the dynamics and steady state geometries of *C. flexa* sheets.

In addition to avoiding the complexity of describing surface curvatures H, K in a discrete program, I find the force equations are relatively quite tractable. Expressing the gradient of the energy as summations over collars belonging to each cell or cell-cell interactions makes it possible to neatly arrange the force calculations as tensor index contractions or, even more simply, matrix multiplications. Of course, describing choanoflagellate sheets as discrete systems also remains faithful to real sheets, and this approach remains applicable over colonies of all cell counts.

3.1   Discrete sheet description

The most natural framework to describe a interactions between a set of discrete points is graph theory. Since colonies of *C. flexa* form sheets with two distinct sides and there is no evidence to suggest that *Choanoeca* acts otherwise [3, 14], we are welcome to treat the

---

[1]in this case, cells

network of interactions between cells as a plane graph G. With cells $C = \{\alpha\}_{\alpha \in C}$ making up vertices and cell-cell interactions via collars $E = \{(\alpha, \beta)\}_{(\alpha, \beta) \in E}$ making up edges in G, we describe which cells impart forces on each other.

However, we understand from the studies into *Choanoeca* that cells interact through their collars [7, 14, 3]. Guided by sheet-tangential imaging

> ak2351: reference a figure with Leadbeater [14] 6A and Brunet et al. [3] 5B

, we see that another natural planar graph G^* is that with edges along interfaces between cells' collars. [2] In this description, vertices mark the points at which the interface between a pair of cells $(\alpha, \beta) \in E$ ends. For a cell $\alpha \in C$ whose collar microvilli are all in contact with those of other cells, the vertices in G^* corresponding to cell α are points where α interacts with two or more cells simultaneously.

As each edge in G^* transects an edge (α, β) between cells α, β in G, we identify G^* as the dual graph of G [3] (figure 3.8a). Consequently, we have that either G or G^* is sufficient to specify the topology of the other provided the coordinates of vertices (figure 3.8b).

> ak2351: todo: include here discussion of which descriptions to use. Why do we choose the more complex model with both collar vertices and cell positions?

3.1.1   Numerically specifying initial conditions

For sheets whose graph of cell-cell connections G can be drawn on a plane with edges as straight lines, it is simplest to define the initial spatial graph G as lying in the *xy*-plane with cell coordinates $\{r_\alpha\}_{\alpha \in C}$ and to use Voronoi tessellation to generate collar vertices in G^*. Voronoi tessellation allows for generalisation beyond regular lattices, though it does not facilitate graph topologies that cannot be drawn in a plane as described above.

To build more complex graphs G that are nevertheless planar, we can either use subsets of common polyhedra (e.g. subdivided icosahedron) or triangulate points that lie along a surface. In the latter case, I found sufficient flexibility in randomly sampling a specified number of points uniformly distributed on a sphere below some latitude, then calculating

---

[2] Until noted otherwise, I treat the several collars interacting between two cells as a continuous line of interaction with infinitesimal collars spanning the cells' interface. The implications of this choice are discussed later.

[3] As G is finite, all vertices in G^* as described above which indicate two cells' interactions ending at the edge of a colony sheet would be merged into a single vertex v_* in the dual graph of G. Consequently G^* is not exactly the dual graph of G. We address this later when defining sheet edges numerically by replacing each edge (v, v^*) in G^* with the edge (v, v') for new vertices v' and removing v_* from G^* and deleting all edges incident on v_*.

the generalised Voronoi tessellation with respect to the metric on the sphere as described in

Caroli et al. [4].

ak2351: add a figure showing the various initial conditions

We build introduce vertices from G^* where two cells' collar microvilli diverge to build a larger graph $\mathfrak{G}$ consisting of cell-cell interaction edges (α, β) from G and cell-collar edges (α, ρ) between cells α and collar edges $\rho \in \alpha$. Here, $\rho \in \alpha$ denotes a collar vertex ρ from G^* connecting to cell α via the cell's microvilli. With cell positions r_α already specified and cell-cell interactions given from G, collar vertex positions r_ρ of collar vertices connecting to three cells are initially set as the centroid of the three cells plus the normal vector of the triangle they form. The orientation of the normal vector is set to be consistent across the sheet, such that all collar vertices are positioned on the same side of the sheet, as all cells in *C. flexa* colonies face the same direction.[4]

As Voronoi diagrams for finitely many cells include ridges that extend out to infinity, and the spherical Voronoi algorithm on points below a given latitude on the sphere produces ridge vertices above that latitude, collar vertices at the boundary of the sheet must be added manually. I call these collar vertices at the edges as *boundary collars*. Before choosing to add these vertices, we must first consider how collar interactions at the boundary affect sheet energy.

Boundary collar vertices

We ask whether boundary collar vertices contribute to the energy. For boundary cells α, β, suppose the line of physical interactions between the two cells' microvilli spans from point r_ρ and ends at point r_σ. We with to know how the angle between the planes given by points ρ, α, σ and ρ, β, σ changes with the position of boundary collar vertex σ.

Suppose for the time being that the collar length is fixed at ℓ, so the possible values for r_σ are constrained. We simplify the problem by reparameterising our coordinates such that $r_\alpha = (-1, 0, 0)$, $r_\rho = (0, r, 0)$, and $r_\beta = (1, 0, 0)$, where $r = \sqrt{\ell^2 - 1}$. Here, ℓ is a dimensionless ratio of the collar length to half the cell-cell distance. We readily see that $r_\sigma = (x, y, z)$ is constrained to take values in the circle defined by $r^2 = y^2 + z^2, x = 0$.

Parameterising the positions of $r_\sigma(\theta) = (0, r\cos\theta, r\sin\theta)$ by angle θ with the second axis, we find the normals for planes ρ, α, σ and ρ, β, σ as

---

[4]Since I use Voronoi triangulation to collar vertices, at most three cells interact at any collar vertex. This is a consequence of the dual of Voronoi tesselation being Delaunay triangulation.
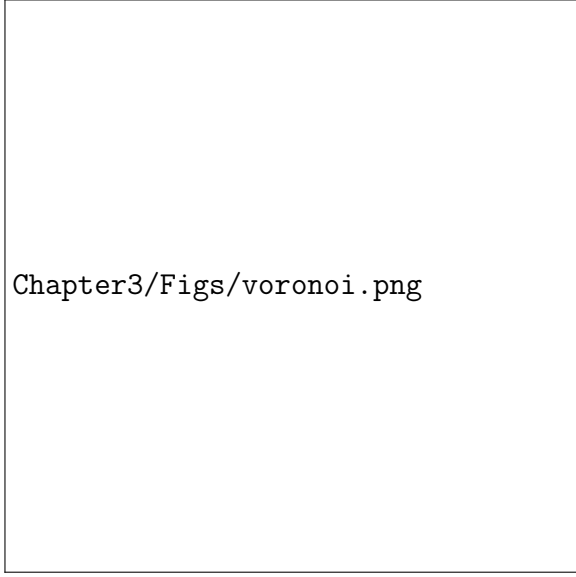
Fig. 3.1 Voronoi tesselation of initial cell placement. Cell bodies shown in blue points, collar boundaries shown in black lines with collar boundary end points shown in orange. Notably, the regions corresponding to boundary cells extend out to infinity. We need to add all boundary collar vertices along the infinite dashed lines.

$$\hat{\boldsymbol{n}}_{\rho\alpha\sigma} = (\boldsymbol{r}_\sigma - \boldsymbol{r}_\alpha) \times (\boldsymbol{r}_\rho - \boldsymbol{r}_\alpha)$$

$$= \frac{(-r^2 \sin\theta, r\sin\theta, r - r\cos\theta)}{r^4 \sin^2\theta + 2r^2(1 - \cos\theta)}$$

$$\hat{\boldsymbol{n}}_{\rho\beta\sigma} = (\boldsymbol{r}_\rho - \boldsymbol{r}_\beta) \times (\boldsymbol{r}_\sigma - \boldsymbol{r}_\beta)$$

$$= \frac{(r^2 \sin\theta, r\sin\theta, r\cos\theta - r)}{r^4 \sin^2\theta + 2r^2(1 - \cos\theta)}.$$

After simplifying, the angle between these two normal vectors is

$$\hat{\boldsymbol{n}}_{\rho\alpha\sigma} \cdot \hat{\boldsymbol{n}}_{\rho\beta\sigma} = 1 - \frac{2}{1 + \frac{1}{2r^2}\left(1 + \tan^2\frac{\theta}{2}\right)}. \tag{3.1}$$

It is clear that the position of the boundary collar interaction at $\boldsymbol{r}_\sigma$ changes the angle between these two planes, given by the arccosine of equation (3.1). In the simplified sheet structure defined in the combined cell-collar graph $\mathfrak{G}$, this results in a change in energy based on the position of $\boldsymbol{r}_\sigma$. Consequently, as the notation indicates, boundary collar vertices are introduced to $\mathfrak{G}$ connecting between each pair of boundary cells.

Adding boundary collar vertices   1

Defining initial positions for boundary collar vertices becomes challenging when sheets are   2
not planar, though a reasonable placement is sufficient since the positions will be changed   3
later. For sheets in the *xy*-plane generated by 2-dimensional Voronoi tesselation (figure 3.1),   4
ridges extending out to infinity are removed and replaced with collar vertices at finite distance.   5
The position of a boundary collar vertex σ between cells α, β is calculated as follows. First,   6
a unit vector $\hat{\boldsymbol{n}}$ perpendicular to the ridge between cell positions $\boldsymbol{r}_\alpha, \boldsymbol{r}_\beta$ is determined. For   7
sheets in the *xy*-plane, $\hat{\boldsymbol{n}} = \hat{z}$. Otherwise, $\hat{\boldsymbol{n}}$ is simply aligned with the average of the normal   8
vectors $\hat{\boldsymbol{n}}_\alpha, \hat{\boldsymbol{n}}_\beta$. Then, the boundary collar vertex position $\boldsymbol{r}_\sigma$ is positioned at the reflection of   9
$\boldsymbol{r}_\rho$ over the plane given by points $\boldsymbol{r}_\alpha, \boldsymbol{r}_\beta, \boldsymbol{r}_\alpha + \hat{\boldsymbol{n}}$, where ρ is the existing collar vertex shared   10
by α and β. Notably, this process results in a boundary collar position $\boldsymbol{r}_\sigma$ farther from the   11
center of the sheet than $\boldsymbol{r}_\rho$ and equidistant to $\boldsymbol{r}_\alpha, \boldsymbol{r}_\beta$ as $\boldsymbol{r}_\rho$.   12

This process produced reasonable boundary collar vertex positions to initialise sheet   13
dynamics simulations (figure 3.2). For initial collar positions not too far from cells, collars   14
did not overlap or cross over each other. Some initial graphs $\mathfrak{G}$ are shown projected onto the   15
xy-plane, though the collars are offset in *z* (**??**) or the entire sheet is not necessarily lying in   16
the *xy*-plane (**??**).   17

> ak2351: add to figure 3.2   18

3.2   Sheet energy   19

In developing the simplified, discrete model for *C. flexa* as a spatial graph, I aim to distill the   20
complex physics of collar-collar interactions into a minimum number of sufficient energy   21
terms to capture the sheet bending that we observe experimentally. In what follows, I treat   22
edges (α, ρ) between a cell α and collar vertex ρ as straight line collar microvilli and cell   23
pairs, flanking collar pairs $(\alpha, \beta : \rho, \sigma)$ as lines of interactions between the planes given by   24
points ρ, α, σ and ρ, β, σ.   25

Consequently, as detailed in the continuous model description of chapter 2, I build an   26
energy function $\mathscr{E}$ that penalises deviations for angles ϕ and ψ, which describe angles   27
between (ϕ) collar microvilli and cell normal vectors $\hat{\boldsymbol{n}}_\alpha$ and (ψ) plane normals $\hat{\boldsymbol{n}}_{\rho\alpha\sigma}, \hat{\boldsymbol{n}}_{\rho\beta\sigma}$.   28

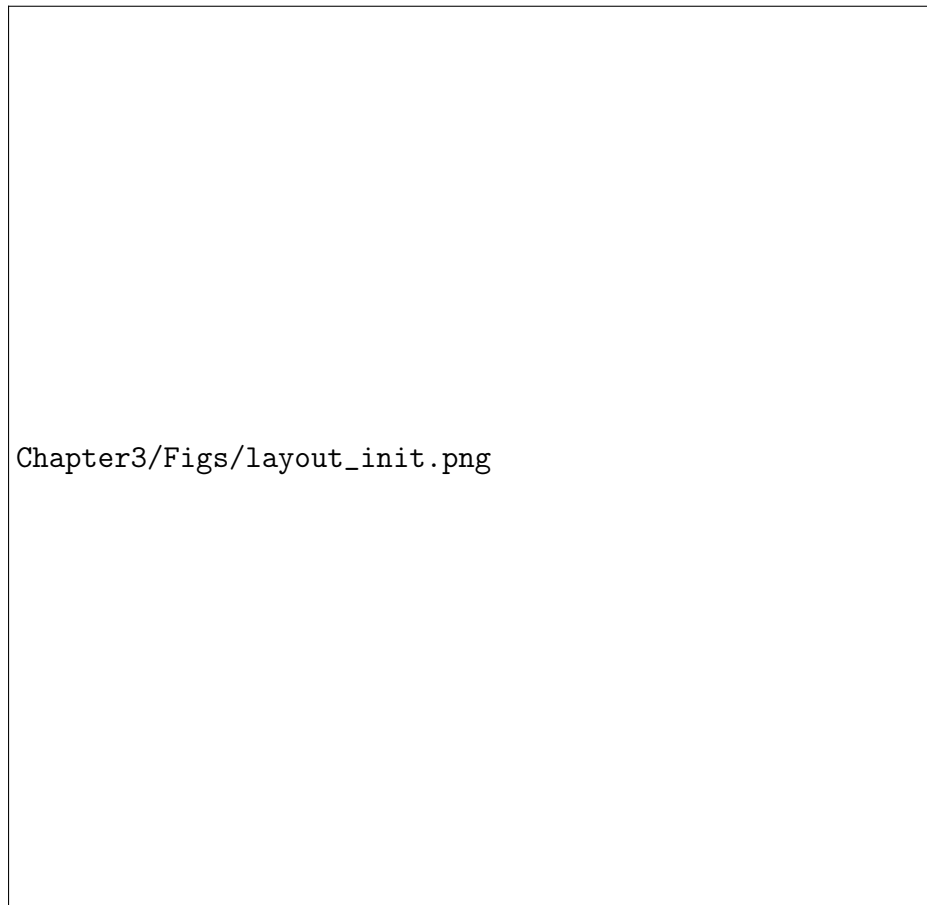Chapter3/Figs/layout_init.png

Fig. 3.2 Initial layout for the flexa sheet. Cell bodies are shown in large purple points and collar boundary vertices are shown in small yellow points. Black edges connect cells to collar boundary vertices, and orange edges show cell-cell neighbor relations (though these orange edges are not physically present). The physical interactions are mediated through the black edges.

3.2.1   Cell-collar angle energy

Cell normal definition

For a physical *C. flexa* cell α with fixed position $\boldsymbol{r}_\alpha$ and fixed collar positions $\{\boldsymbol{r}_\rho\}_{\rho \in \alpha}$, we realise that the cell still has freedom in its rotation which we expect will contribute substantially to its energy. In other words, there should be an optimal rotation for the cell to minimise its mechanical energy. Since we treat *C. flexa* cells as rotationally symmetric above the apicobasal axis, it suffices in our description to assign to each cell α in the graph $\mathfrak{G}$ a unit vector $\hat{\boldsymbol{n}}_\alpha$

For simplicity, each vector $\hat{\boldsymbol{n}}_\alpha$ is initially defined as the unit vector in the direction of $\sum_{\rho \in \alpha} \vec{\alpha\rho}$, where $\vec{\alpha\rho} = \boldsymbol{r}_\rho - \boldsymbol{r}_\alpha$.

Energy $\mathscr{E}_\phi$

Defining an energy term on the angle ϕ between a cell α's collars and the apicobasal axis $\hat{\boldsymbol{n}}_\alpha$ is established on descriptions of *Choanoeca* in the literature. Brunet et al. [3] describes the change in this angle as the result of exposure to light in *C. flexa*. Similarly, Ellis [7] characterises the variation in ϕ observed in individual cells of *C. perplexa*.

Consequently, we consider an energy term $\mathscr{E}_\phi(\{\boldsymbol{r}_\alpha, \hat{\boldsymbol{n}}_\alpha\}, \{\boldsymbol{r}_\rho\})$ which penalises devation from a common equilibrium basal collar angle ϕ_0:

$$\mathscr{E}_\phi(\{\boldsymbol{r}_\alpha, \hat{\boldsymbol{n}}_\alpha\}, \{\boldsymbol{r}_\rho\}) = \sum_{(\alpha, \rho)} \left(\phi_{(\alpha, \rho)} - \phi_0\right)^2. \tag{3.2}$$

The sum indicates summation over all cell-collar pairs (α, ρ) in the sheet $\mathfrak{G}$. The angle $\phi_{(\alpha, \rho)}$ is calculated entirely based on the cell normal vector $\hat{\boldsymbol{n}}_\alpha$ and unit vector $\hat{\vec{\alpha\rho}}$ pointing in the direction of $\hat{\boldsymbol{r}}_\rho - \hat{\boldsymbol{r}}_\alpha$:

> ak2351: make this equation numbered and number other substantial equations

$$\phi_{(\alpha, \rho)} = \arccos\left(\hat{\boldsymbol{n}}_\alpha \cdot \hat{\vec{\alpha\rho}}\right) = \arccos\left(\hat{\boldsymbol{n}}_\alpha \cdot \frac{\vec{\alpha\rho}}{|\vec{\alpha\rho}|}\right).$$

Optimal cell normal vectors

No other energy terms will depend on the cell normal vectors $\{\hat{\boldsymbol{n}}_\alpha\}$, so we ask now what the optimal normal vector for a cell is. Suppose a cell is at position $\boldsymbol{r}_\alpha$ with collar vertices at $\boldsymbol{r}_\rho$

1   for $\rho \in \alpha$. We can determine how the cell orients in order to minimise the collar energy with

2   respect to $\hat{\boldsymbol{n}}_\alpha$.

3   For fixed α, the cell orientation vector $\hat{\boldsymbol{n}}_\alpha$ is constrained to have unit length. Hence, we

4   solve the constrained optimisation of $\mathscr{E}_\phi$ by solving the Lagrange multiplier problem with

5   multiplier λ

$$0 = \frac{\partial \left[\mathscr{E}_\phi \lambda \left(|\hat{\boldsymbol{n}}_\alpha|^2 - 1 \right) \right]}{\partial \hat{\boldsymbol{n}}_\alpha} \tag{3.3}$$

$$0 = \frac{\partial \left[\mathscr{E}_\phi + \lambda \left(|\hat{\boldsymbol{n}}_\alpha|^2 - 1 \right) \right]}{\partial \lambda}. \tag{3.4}$$

9   Using the constraint (solution to equation (3.4)) $|\hat{\boldsymbol{n}}_\alpha|^2 = 1$, we solve

$$\lambda \hat{\boldsymbol{n}}_\alpha = 2 \sum_{\rho \in \alpha} \left[\arccos \left(\hat{\alpha\rho} \cdot \hat{\boldsymbol{n}}_\alpha \right) - \phi_0 \right] \frac{-1}{\sqrt{1 - \left(\hat{\alpha\rho} \cdot \hat{\boldsymbol{n}}_\alpha \right)^2}} \hat{\alpha\rho}$$

$$\lambda = 2 \left| \sum_{\rho \in \alpha} \left[\arccos \left(\hat{\alpha\rho} \cdot \hat{n}_\alpha \right) - \phi_0 \right] \frac{1}{\sqrt{1 - \left(\hat{\alpha\rho} \cdot \hat{n}_\alpha \right)^2}} \hat{\alpha\rho} \right|.$$

13 Then the optimal normal vector solves the transcendental equation

$$\hat{\boldsymbol{n}}_\alpha = \frac{\sum_{\rho \in \alpha} \left[\arccos \left(\hat{\alpha\rho} \cdot \hat{\boldsymbol{n}}_\alpha \right) - \phi_0 \right] \frac{-1}{\sqrt{1 - (\hat{\alpha\rho} \cdot \hat{\boldsymbol{n}}_\alpha)^2}} \hat{\alpha\rho}}{\sum_{\rho \in \alpha} \left[\arccos \left(\hat{\alpha\rho} \cdot \hat{\boldsymbol{n}}_\alpha \right) - \phi_0 \right] \frac{1}{\sqrt{1 - (\hat{\alpha\rho} \cdot \hat{\boldsymbol{n}}_\alpha)^2}} \hat{\alpha\rho}} \tag{3.5}$$

16   Clearly the cell normal vectors must be computed numerically whenever a cell is inter-

17 acting with several other cells simultaneously in complicated geometries. We can choose to

18 either approximate the normal vectors with a physically reasonable approximation or treat

19 the normal vectors as free arguments to the energy function to be optimised. I discuss both

20 options below.

Approximating cell normal vectors

22 There are several options for approximating a cell normal vector $\hat{\boldsymbol{n}}_\alpha$ based on positions $\boldsymbol{r}_\alpha$

23 and $\{\boldsymbol{r}_\rho\}_{\rho \in \alpha}$. The simplest option we might be able to think of is to let $\hat{\boldsymbol{n}}_\alpha$ be the unit

vector in the direction $\sum_{\rho \in \alpha} \hat{\alpha\rho}$. This approach has the benefit that collar vertices farther from $\boldsymbol{r}_\alpha$ are weighted more in the cell normal vector, agreeing with the intuition that a more distant collar interaction demands more cell rotation to accommodate it. However, we find that this approach results in unreasonable cell normal vectors for boundary cells as defined in $\mathfrak{G}$ since boundary cells do not have a full ring of boundary collar vertices. For this approach to work, $\mathfrak{G}$ would need to include several more collar vertices which do not describe interactions between cells and add unnecessary complexity. In application, I found that the boundary cell effect of this choice of $\hat{\boldsymbol{n}}_\alpha(\boldsymbol{r}_\alpha, \{\boldsymbol{r}_\rho\}_{\rho \in \alpha})$ substantially affected boundary collar vertex positions after energy equilibration and the overall energy landscape as a function of equilibrium angles ϕ_0, ψ_0.

When initialising a flat sheet, the above averaging approach also does not agree with intuition, since it results in boundary cell normal vectors that do not point in the same direction as normal vectors for cells not on the sheet boundary (figure 3.2). Instead, when a sheet lies flat in the xy-plane, it is expected that all vectors $\hat{\boldsymbol{n}}_\alpha$ point in the $+\hat{z}$ direction provided that collars are above cells in $\boldsymbol{z}$. A viable alternative is to define $\hat{\boldsymbol{n}}_\alpha$ by taking a plane approximation to cell α's collar vertices. The normal vector to this plane oriented away from the cell defines a normal vector that agrees with intuition and supports calculating normals for a non-coplanar set of collar vertices.

The plane approximation approach is easiest achieved using ordinary least squares. Briefly, we approximate $\hat{r}_{\rho 3} = (r_{\rho 1}, r_{\rho 2}) \cdot (\beta_1, \beta_2) + \beta_0$ and minimise the sum of squared residuals $\sum_{\rho \in \alpha} (\hat{r}_{\rho 3} - r_{\rho 3})^2$ with respect to $\beta_0, \beta_1, \beta_2$. The normal vector of the plane approximation is then $(\beta_1, \beta_2, -1)$ up to normalisation and multiplication by -1.[5]

3.2.2   Cell-cell junction angle ψ energy

As in chapter 2, we aim to produce sheet curvature with the angle ψ that two cells' collars make at their interface. As in section 3.1.1, we calculate the angle between planes defined by two cells α, β and their mutual flanking collar vertices ρ, σ with

$$\psi_{(\alpha,\beta:\rho,\sigma)} = \frac{\pi}{2} - \frac{1}{2}\arccos\left(\hat{\boldsymbol{n}}_{\rho\alpha\sigma} \cdot \hat{\boldsymbol{n}}_{\rho\beta\sigma}\right) \tag{3.6}$$

The normal vectors $\hat{\boldsymbol{n}}_{\rho\alpha\sigma}$ for a plane given by points ρ, α, σ must have a systematically defined orientation, as they can point in either direction $\pm(\boldsymbol{r}_\rho - \boldsymbol{r}_\alpha) \times (\boldsymbol{r}_\sigma - \boldsymbol{r}_\alpha)$. In the

---

[5]The notation here is chosen to be consistent with that typically used in ordinary least squares, hence the hatted values indicate an approximation rather than vector normalisation as I use otherwise.

¹ geometry used to define ψ in equation (3.6), the collar-cell-collar normal vectors are assumed

² to be pointing in the direction of the cells' flagella. With the simplifying assumption that

³ the cell normal always points in the inside of the collar, we have that the collar-cell-collar

⁴ normals must take orientation to align with their corresponding cell normals. Consequently,

⁵ we let $\hat{\boldsymbol{n}}'_{\rho\alpha\sigma} = \vec{\alpha\rho} \times \vec{\alpha\sigma}$ and set $\hat{\boldsymbol{n}}_{\rho\alpha\sigma} = \mathrm{sgn}(\hat{\boldsymbol{n}}'_{\rho\alpha\sigma} \cdot \hat{\boldsymbol{n}}_\alpha)\hat{\boldsymbol{n}}'_{\rho\alpha\sigma}.$[6]

⁶   Defining $\hat{\boldsymbol{n}}_{\rho\alpha\sigma}$ in this way makes it dependent on the cell normal vectors $\hat{\boldsymbol{n}}_\alpha$. However,

⁷ when minimising the energy, I work to develop methods such that $\mathrm{sgn}(\hat{\boldsymbol{n}}_{\rho\alpha\sigma} \cdot \hat{\boldsymbol{n}}_\alpha)$ remains

⁸ constant. This corresponds to ensuring that no collar vertices cross through each other

⁹ (corresponding to microvilli crossing over each other) and that the cell normal vectors remain

¹⁰ pointing inside the collars. Hence, I effectively treat the effect of $\hat{\boldsymbol{n}}_\alpha$ on a collar-cell-collar

¹¹ normal vector $\hat{\boldsymbol{n}}_{\rho\alpha\sigma}$ to be constant.

¹²   With a common equilibrium collar-collar interface angle ψ_0 (as all cells are assumed

¹³ equal in their mechanical properties), we express the energy $\mathscr{E}_\psi$

$$\mathscr{E}_\psi = k_\psi \sum_{(\alpha,\beta:\rho,\sigma)} \left(\psi_{(\alpha,\beta:\rho,\sigma)} - \psi_0\right)^2. \tag{3.7}$$

3.2.3   Collar length

¹⁷ To provide sufficient flexibility to sheets through collar microvilli, I introduce an energy term

¹⁸ $\mathscr{E}_{\mathrm{sp}}$ defined by

$$\mathscr{E}_{\mathrm{sp}} = k_{\mathrm{sp}} \sum_{(\alpha,\rho)} \left|\vec{\alpha\rho} - \ell_{0\alpha\rho}\right|^2, \tag{3.8}$$

²¹ where $\ell_{0\alpha\rho}$ is an equilibrium length for edge (α,ρ). The sum indicates summation over all

²² cell, collar pairs (α,ρ) in the sheet $\mathfrak{G}$.

²³   All cells are assumed to take identical properties, so all values $\ell_{0\alpha\rho}$ are set to a constant

²⁴ ℓ_0 unless indicated otherwise. When done so, we find that ℓ_0 is the only length defined in the

²⁵ problem.

²⁶   When interested in sheets with constrained collar length, we may either take a numerical

²⁷ approach or exploit the above energy term by setting k_{sp} to a large value. The former is

²⁸ discussed in section 3.7.2.

---

[6]Here sgn is the sign operator.

3.3 Minimising sheet energy

We now have an energy $\mathscr{E}\{r_v\}_{v\in\mathfrak{G}} = \mathscr{E}_\phi + \mathscr{E}_\psi$ which is parameterised over the cell and collar boundary vertex positions. Notably, we treat the topology of the network as fixed, so the indices of the summations for $\mathscr{E}_\phi$ and $\mathscr{E}_\psi$ are unchanged even as we minimise energy.

Flat sheet as a solution

Notice that we have a pair (ϕ_0, ψ_0) that gives $\mathscr{E} = \mathscr{E}_\phi + \mathscr{E}_\psi = 0$. Since the ϕ and ψ energies are nonnegative, the flat sheet is a stable minimum.

Constant collar length constraint

For now, we are numerically constraining the cell-collar lengths at ℓ, their initial lengths (which are constant for all cells). If we want to use the generalisability of our model to use an random initial cell distribution and generate the irregular boundaries with Voronoi tesselation, we will have to relax this condition and add a collar length spring energy to $\mathscr{E}$. The constant collar length constraint only applies to sheets generated by regular lattices when laid flat on a plane.

The constraint is defined by a vector function $f((c,b)) = |r_c - r_b| - \ell = 0$ for all cell-collar edges (c,b). If n_{collars} is the number of cell-collar edges in {cell-collar edges (c,b)}, then f defines a n_{collars}-vector function.

My optimisation routine requires that we calculate a Jacobian matrix for the vector constraint function. This gets ugly if we use f as written above, but it is fortunately equivalent to set the constraint $f'((c,b)) = |r_c - r_b|^2 - \ell^2 = 0$. It is an interesting problem to take the gradient of f' with respect to all of the coordinates, but I won't include it here. It's implemented in my code.

Solving sheet shape

Numerical optimisation: sensitivity issues and initial conditions

    Derive the gradient

    Describe how to compute the gradient in an efficient way

3.3.1   Graph topology

For hexagonal lattice start, we

    Call back to section 2.1

3.4   Energy gradient descent

Due to the instability of the numerical optimisation routine used above, I moved to minimising the total energy $\mathscr{E}$ explicitly using gradient descent. The goal in taking this approach is to explicitly calculate the gradients $\partial\mathscr{E}/\partial\boldsymbol{r}_\gamma$ of the energy with respect to all coordinate vectors $\boldsymbol{r}_\gamma$ and incrementally take small steps in the reverse direction.

    Although gradient descent in several contexts is criticised for being slow and by nature prone to be trapped in local minima, in the context of modeling *C. flexa* sheets it is preferable to a black box optimisation routine. Calculating the gradient analytically amounts to calculating the forces on all coordinates, and taking incremental steps in the direction of the negative gradient amounts to forward integrating Newton's laws $F_\gamma = -\partial\mathscr{E}/\partial\boldsymbol{r}_\gamma$. Consequently, we gain access to the dynamics induced by the simplified model that I describe above. Moreover, the susceptibility of this approach to be trapped in local minima is ideal not only from an energetic perspective, but also from a numerical one: by taking incremental steps in a direction known to decrease the energy, any increases indicate a flaw and

> ak2351: and what??

    In contrast to a numerical optimisation routine, gradient descent requires substantial explicit calculation. Moreover, the algorithm requires tuning in the step size and relative decrease in energy tolerance at which to decide the algorithm has terminated.

3.4.1   Deriving the gradient

The linearity of the gradient permits us to take the gradient term-by-term in **??**. For an energy function $\mathscr{E}(\{\boldsymbol{r}_\gamma\})$ with cell normal vectors $\hat{\boldsymbol{n}}_\alpha$ approximated in terms of each cell's collar vertices, we find that the gradient $\partial\mathscr{E}_\phi/\partial\boldsymbol{r}_\gamma$ is given by

$$phieq \tag{3.9}$$

> ak2351: describe how this can be simplified as a matrix mult problem

As discussed in 3.2.2, an angle $\psi_{(\alpha,\beta:\rho,\sigma)}$ for a cell-cell interface depends in a piecewise   1
constant way on the cells' normal vectors. While the angles are consequentially only   2
piecewise differentiable, gradient descent makes reasonable the assumption that there will   3
not be any discontinuities in $\mathscr{E}_\psi$ for sufficiently small steps in the direction of the negative   4
gradient. The below expression for $\partial\mathscr{E}_\psi/\partial\boldsymbol{r}_\gamma$ assumes that the sign of $\hat{\boldsymbol{n}}_\alpha \cdot (\vec{\alpha\rho} \times \vec{\alpha\sigma})$ 5
remains constant.   6

$$psieq \tag{3.10}$$ 7
    8

The gradient $\partial\mathscr{E}_{\mathrm{sp}}/\partial\boldsymbol{r}_\gamma$ is given by the linear spring force   9

$$springeq \tag{3.11}$$ 10
    11

3.4.2   Forward integration   12

Integrating the gradient given by equations equations (3.9) to (3.11) produces the dynamics   13
of sheet bending as in figure 3.3.   14

ak2351: discuss the equilibrium states   15

$$\boldsymbol{r}_\gamma(t+\Delta t) = \boldsymbol{r}_\gamma(t) - \Delta t \frac{\partial\mathscr{E}}{\partial\boldsymbol{r}_\gamma}. \tag{3.12}$$ 16
    17

When treating the normal vectors $\hat{\boldsymbol{n}}_\alpha$ as free variables, we must solve modify our force   18
equilibration algorithm to maintain the constraint that $|\hat{\boldsymbol{n}}_\alpha|^2 = 1$. An intuitive option is to   19
step in the direction of the negative gradient and normalise the intermediate vectors at each   20
step: 21

$$\boldsymbol{n}_\alpha(t+\Delta t) = \hat{\boldsymbol{n}}_\alpha(t) - \Delta t \frac{\partial\mathscr{E}}{\partial\hat{\boldsymbol{n}}_\alpha} \tag{3.13}$$ 22

$$\hat{\boldsymbol{n}}_\alpha(t+\Delta t) = \frac{\boldsymbol{n}_\alpha(t+\Delta t)}{\boldsymbol{n}_\alpha(t+\Delta t)}. \tag{3.14}$$ 23
    24

Equivalently, since for a sufficiently small step size the nearest point on the constraint   25
set $|\hat{\boldsymbol{n}}_\alpha|^2 = 1$ to $\boldsymbol{n}_\alpha(t+\Delta t)$ is unique, we may re-express equation (3.14) with $\hat{\boldsymbol{n}}_\alpha(t+\Delta t) =$ 26

Fig. 3.3 todo

$\arg\min_{|\hat{\boldsymbol{n}}_\alpha|^2=1} |\hat{\boldsymbol{n}}_\alpha - \boldsymbol{n}_\alpha(t+\Delta t)|$. Expressed in this way, we see that the update for $\hat{\boldsymbol{n}}_\alpha$ expressed in equations (3.13) and (3.14) is exactly the projected gradient descent algorithm and we expect it to converge [6]. Since the normal component of $\partial\mathscr{E}/\partial\hat{\boldsymbol{n}}_\alpha$ to the constraint set $|bhn_\alpha|^2 = 1$ at step t does not affect $\hat{\boldsymbol{n}}_\alpha(t+\Delta t)$, we can interpret equations (3.13) and (3.14) as taking a step in the direction of the tangent space to the constraint set that reduces $\mathscr{E}$ the most.

> ak2351: discuss the dynamics

While the forward integration works well for small sheets with simple graph topologies, I found that some equilbrium angles ϕ_0, ψ_0 caused the sheet to strain to such an extreme that collar vertices would cross through each other. The resulting increase in energy comes from the discontinuous sign function in the definition of ψ (equation (3.6)), and collar vertices cross over each other due to too large of a step size Δt. While adaptively decreasing the step size is a viable option, it would substantially slow the equilibration algorithm. Instead, I introduced an additional term to the energy $\mathscr{E}_\varphi$ based on the angles $\varphi_{\rho\alpha\sigma}$ formed by each cell α and its adjacent pairs of collar vertices ρ, σ when projected onto the plane defined by the cell normal $\hat{\boldsymbol{n}}_\alpha$ (figure 3.4):

$$\mathscr{E}_\varphi = k_\varphi \sum_{(\alpha,\beta:\rho\sigma)} \left(\varphi_{\rho\alpha\sigma} - \varphi_{0\rho\alpha\sigma}\right)^2, \tag{3.15}$$

where $\varphi_{0\rho\alpha\sigma}$ is an equilibrium projected collar-cell-collar angle for each triple. Each angle $\varphi_{0\rho\alpha\sigma}$ is set to the actual value that is evaluated at the initial sheet geometry. Unless specified otherwise, the constant k_φ is set to $0.01k_\phi$.
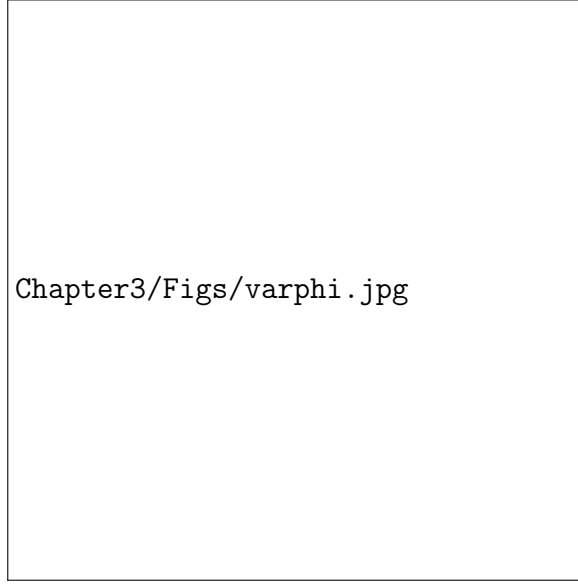
The angles $\varphi_{\rho\alpha\sigma}$ are calculated similarly to ϕ, ψ (**??** and equation (3.6),

$$\varphi_{\rho\alpha\sigma} = \arccos\left[\vec{\alpha\rho}_\parallel \cdot \vec{\alpha\sigma}_\parallel\right], \tag{3.16}$$

where $\vec{\alpha\rho}_\parallel$ is the projection of $\vec{\alpha\rho}$ onto the plane defined by normal $\hat{\boldsymbol{n}}_\alpha$ and position $\boldsymbol{r}_\alpha$.

> ak2351: give formula for $\vec{\alpha\rho}_\parallel$

The gradient of $\mathscr{E}_\varphi$ is given by

Fig. 3.4 Geometry for calculating $\varphi_{\rho\alpha\sigma}$.

$$varphieq \tag{3.17}$$

3.4.3   Exploring the energy landscape

With the ability to study discrete sheet equilibrium geometries and dynamics, we are prepared to evaluate a mechanism for *C. flexa* folding and inversion. Based on the two collar angle states observed in Brunet et al. [3], a reasonable model would be to assume relaxed-state equilibrium angles $\phi_{\text{in}}, \psi_{\text{in}}$ and a different set of active-state angles $\phi_{\text{out}}, \psi_{\text{out}}$ with instantaneous transition between the two states. The rapid change in individual cell behavior and expected gradual sheet shape change expected from opposing cell-cell interactions align with our expectations from observations Brunet et al. [3].

Although we cannot access true values for the equilibrium angles, modeling *C. flexa* sheets numerically provides the opportunity to explore the entire energy landscape. For sheets generated with a regular hexagonal lattice, we observe the expected diagonal valley where energy in minimised in the energy landscape since the sheet is expected to be flat along those pairs (ϕ_0, ψ_0) (figure 3.5). Substantial sheet deformation and bending is evidently not sufficient to overcome the change in terms in the energy function. The increases in energy when the equilibrium angles are most disparate can be interpreted as collar microvilli stretching or compressing to accommodate sheet bending or a difference in the bending at
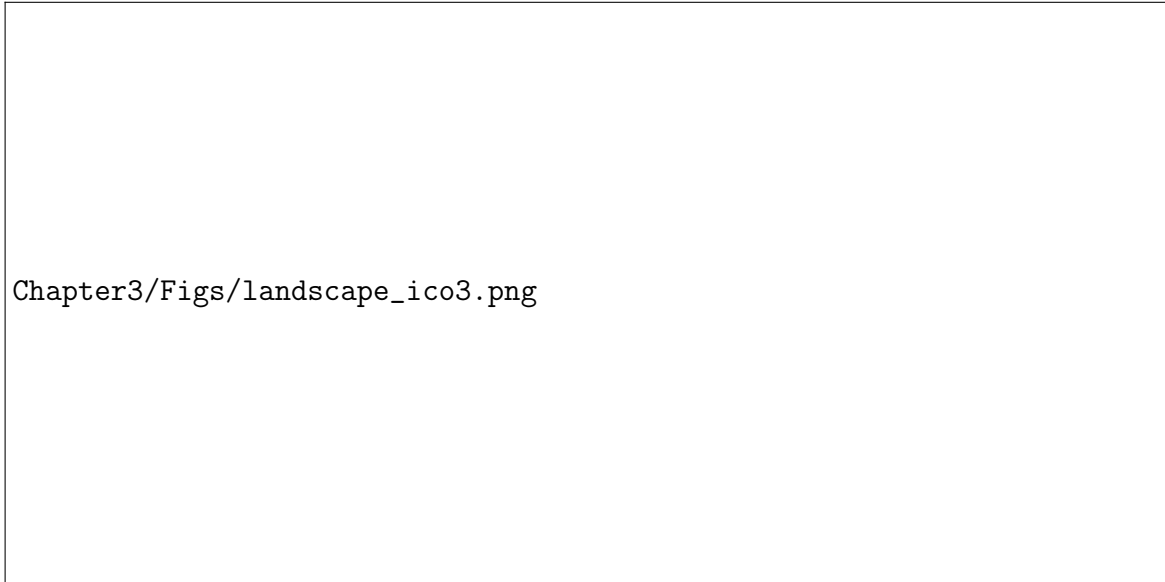
Fig. 3.5 Energy landcsape of a discrete *C. flexa* sheet generated from a hexagonal lattice. Sheets displayed at the right correspond to the corners of the landscape indicated with white crosses.

each cell from the preferred state. For example, cells at neither the centre nor boundary in a bent sheet (figure 3.5, bottom-right or top-left) must contribute a positive contribution to $\mathscr{E}$ since they do not have the symmetric bending at all collar microvilli prescribed by equations (3.2), (3.7) and (3.8).

For graph topologies generated with an icosphere, we observe a more rich energy landscape (**??**). Again we observe a similar minimum energy well running along a diagonal, though the energy increases at the ends since the network of cell-cell connections is not able to accommodate stretching and compression as readily as a sheet generated from a lattice. Notably, the energy well for flagella-out sheets occurs in the region of high ϕ and low ψ. As predicted by equation (2.8), $\phi > \psi$ results in a preferred curvature corresonding to a flagella-out sheet, in agreement with the observed energies. Similarly, we see at these extremely disparate equilibrium angles that the edge of the flagella-in sheet begins to curve outward. The fact that the equilibrium sheet demonstrates this stress indicates that inversion is constrained as a result of cell-cell connections and the collar stiffness k_{sp}.
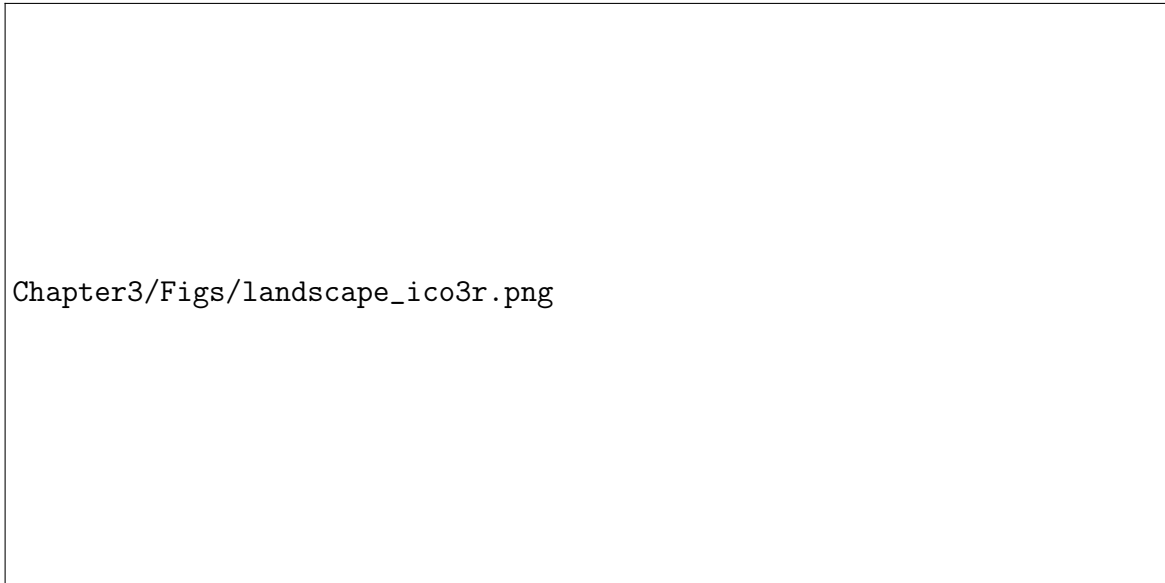
For low ψ and increasing ϕ in figure 3.6a, there appear to be sudden jumps in the energy profile. When investigated, it emerges that these jumps are the result of buckling at the sheet edges, where an increase in ϕ prompts boundary cells that wrap inward (figure 3.6a, bottom left) to push each other outward.

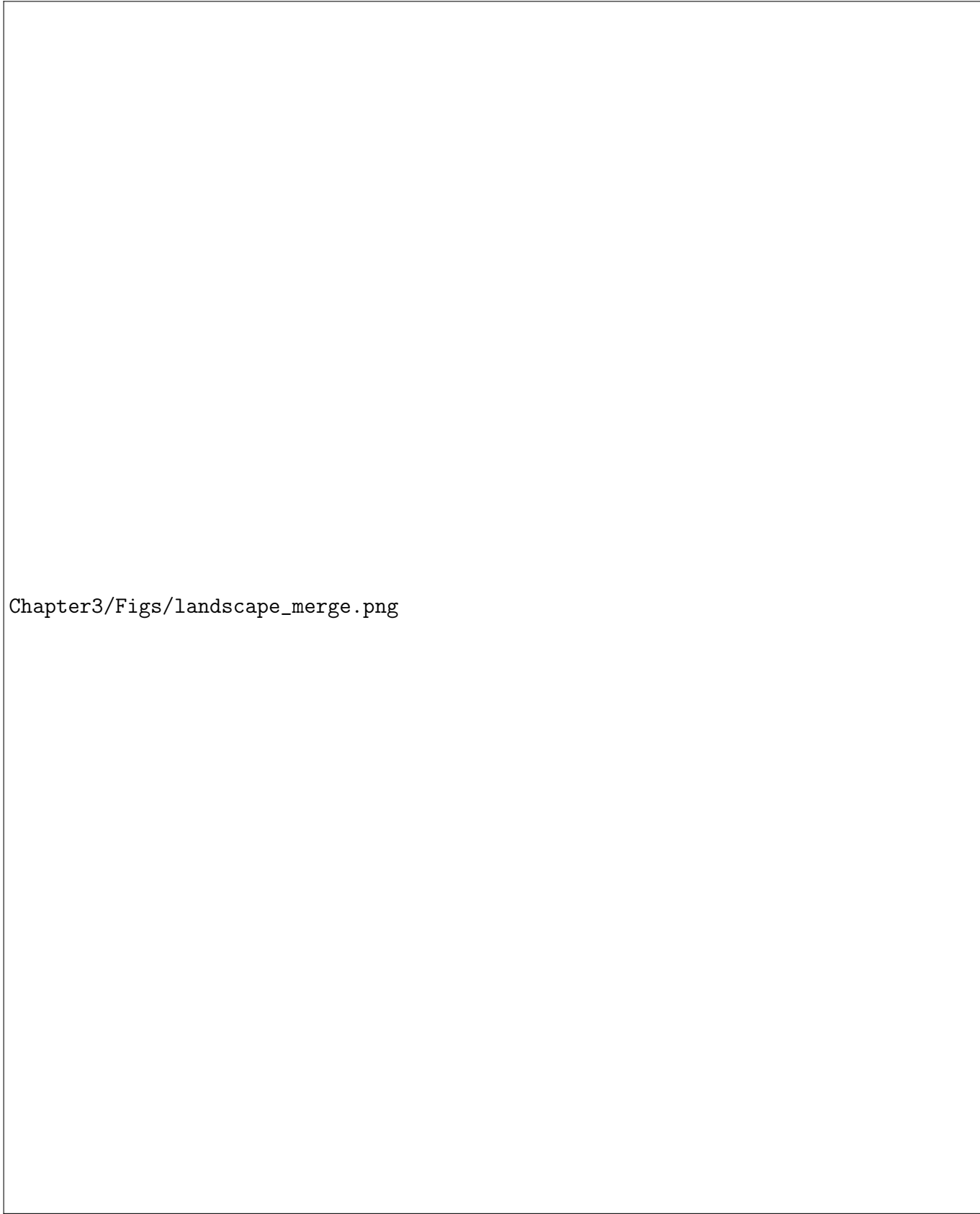ak2351: get ico to invert for small sheets

(a)

(b)

Fig. 3.6 Energy landscapes for (3.6a) flagella-in and (3.6b) flagella-out sheets of *C. flexa*. The color scaling is the same in both images. The landscapes for a smaller segment of the icosphere were qualitatively similar.

As we are interested in the bistability and transition in *C. flexa* sheets, we are concerned with the global energy minima for both flagella-in and -out sheets. In figure 3.7, the minimum energy orientations throughout the landscape of figure 3.6 are shown. As expected, the lowest possible energy can be achieved in the flagella-in orientation, consistent with the belief that cells are relaxed in this state [3]. With an increase in ϕ_0 and decrease in ψ_0, corresponding to constriction in the apical myosin ring and flaring out or stiffening of the collar, the flagella-in state is preferred.

Based on figure 3.7, we are equipped with a reasonable prediction to describe the inversion dynamics of *C. flexa* sheets. A flagella-in sheet at rest with equilibrium angles $\phi_{\text{in}}, \psi_{\text{in}}$ within the energy well of figure 3.6a that immediately changes equilibrium angles to $\phi_{\text{out}}, \psi_{\text{out}}$ may be constrained from inverting due to its collar-collar adhesions. Despite this, the equilibrium angles are fixed as a result of environmental conditions and molecular action within the cells, and inversion relaxes the sheet to decrease energy into the higher yet still energetically preferable well of figure 3.6b.

Despite the favorability of the flagella-out orientation in the active state, it is clear that there is a substantial energetic barrier to reach that state induced by collar-collar adhesion forces and collar stiffness. There is no evidence to suggest changing collar properties, so we are led to predict that changing cell sheet topology is the factor which enables inversion.

$$\vec{F}_\gamma = \frac{\partial E}{\partial \vec{r}_\gamma} = 2 \sum_{(\alpha,\rho)} \left(\phi_{(\alpha,\rho)} - \phi_0\right) \frac{\partial \phi_{(\alpha,\rho)}}{\partial \vec{r}_\gamma} + 2 \sum_{(\alpha,\beta:\sigma,\rho)} \left(\psi(\hat{\boldsymbol{n}}_{\sigma\alpha\rho}, \hat{\boldsymbol{n}}_{\sigma\beta\rho}) - \psi_0\right) \frac{\partial \psi_{(\alpha,\beta:\sigma,\rho)}}{\partial \vec{r}_\gamma}$$

$$\frac{\partial \phi_{(\alpha,\rho)}}{\partial r_{\gamma i}} = \frac{-1}{\sqrt{1 - (\hat{\boldsymbol{n}}_\alpha \cdot (\hat{\alpha\rho}))^2}} \left(\frac{\partial \hat{\boldsymbol{n}}_{\alpha j}}{\partial r_{\gamma i}} (\hat{\alpha\rho})_j + \frac{\partial (\hat{\alpha\rho})_j}{\partial r_{\gamma i}} \hat{\boldsymbol{n}}_{\alpha j}\right)$$

$$\frac{\partial (\hat{\alpha\rho})_j}{\partial r_{\gamma i}} = \frac{(\delta_{\gamma\rho} - \delta_{\gamma\alpha})}{|r_\rho - r_\alpha|} \left(\delta_{ij} + (\hat{\alpha\rho})_i (\hat{\alpha\rho})_j\right)$$

$$\frac{\partial \hat{\boldsymbol{n}}_{\alpha j}}{\partial r_{\gamma i}} = \frac{\mathbb{1}_{\gamma \in \text{collars}(\alpha)} - n\delta_{\gamma\alpha}}{\left|\sum_{(\alpha,\rho)} (r_\rho - r_\alpha)\right|} \left(\delta_{ij} - \hat{\boldsymbol{n}}_{\alpha i} \hat{\boldsymbol{n}}_{\alpha j}\right)$$

$$\frac{\partial \psi_{(\alpha,\beta:\sigma,\rho)}}{\partial r_{\gamma i}} = \frac{-1}{\sqrt{1 - (\hat{\boldsymbol{n}}_{\rho\alpha\sigma} \cdot \hat{\boldsymbol{n}}_{\rho\beta\sigma})^2}} \left(\frac{\partial \hat{\boldsymbol{n}}_{\rho\alpha\sigma j}}{\partial r_{\gamma i}} \hat{\boldsymbol{n}}_{\rho\beta\sigma j} + \frac{\partial \hat{\boldsymbol{n}}_{\rho\beta\sigma j}}{\partial r_{\gamma i}} \hat{\boldsymbol{n}}_{\rho\alpha\sigma j}\right)$$

$$\frac{\partial \hat{\boldsymbol{n}}_{\rho\alpha\sigma j}}{\partial r_{\gamma i}} = \text{too big see notes}$$

Fig. 3.7 Minimum energies the two landscapes shown in figure 3.6. Values pulled from figure 3.6a are denoted with red dots and figure 3.6b with orange dots.

3.5 Everything before written

3.6 Discrete surface model

3.6.1 How to define the surface

We need to determine what parts of our physical problem we will keep track of, and how we will use them to define an energy. There are two natural, physical planar graphs to look at. We could either form the graph with cell bodies forming vertices and edges defined by cells whose collars make contact with each other. Alternatively, vertices could be represented by places where two cells' collars lose contact with each other, and edges could be along the line where those collars contact.

Since these graphs are planar (albeit not necessarily lying along a physical plane), we have a well-defined notion of a graph dual, where each face in one graph corresponds to a vertex in the other. What we find is that the two graphs described above are dual to each other (Figure 3.8a). One graph specifies the topology of the other, but we are considering these as spatial graphs to use their geometries so our problem is not so simple. Knowing the positions of all vertices and knowing the edges of one graph does not give complete information about the other.

Since each cell is identical, we might imagine that the distances between two cells and their mutual boundary is equal. In a loose sense, then, their interactions form a Voronoi tesselation on the surface of collar interactions (with respect to the metric on that surface). We can then take the dual to know that the graph of cell bodies is triangulated, as the dual of a Voronoi tesselation is a Delaunay triangulation (Figure 3.8b).
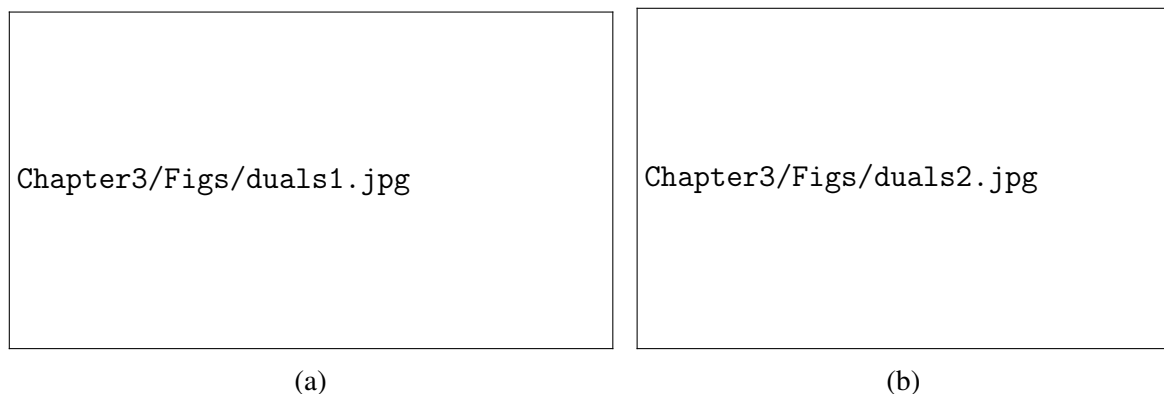

(a)

(b)

Fig. 3.8 Two views of the physical dual graphs used in describing *C. flexa*.

3.6.2   Surface formed by collar boundaries

Stretching

The physical interactions happen at the collar boundaries, so it makes sense to define energy based on the graph that quantifies them. If two cells have a collar boundary described by $\boldsymbol{r_a}t + (1-t)\boldsymbol{r_b}$ with $0 \le t \le 1$ and the energy is defined by continuously many springs from the boundary to a projected cell point $\boldsymbol{r_\Delta}$, then the energy $\mathscr{E}_{ab}$ of that boundary is

$$\mathscr{E}_{ab} = \int_0^1 [(\boldsymbol{r_a}t + (1-t)\boldsymbol{r_b}) - \boldsymbol{r_\Delta}]^2 \, dt = \frac{1}{3}(\boldsymbol{r_a} + \boldsymbol{r_b})^2 - \frac{1}{3}\boldsymbol{r_a} \cdot \boldsymbol{r_b} - \boldsymbol{r_\Delta} \cdot (\boldsymbol{r_a} + \boldsymbol{r_b}) + \boldsymbol{r_\Delta}^2.$$

$$(3.18)$$

The energy corresponding to a cell consists of the line energies of all the collar interfaces. We find the position $\boldsymbol{r_\Delta}$ by setting the gradient of equation 3.18 with respect to $\boldsymbol{r_\Delta}$ to zero for all lines ab. If b indexes the vertices that cell Δ has, then

$$0 = \frac{d\mathscr{E}}{d\boldsymbol{r_\Delta}} = -\sum_{b \in \Delta} \boldsymbol{r_b} + 2n\boldsymbol{r_\Delta}$$

$$\boldsymbol{r_\Delta} = \frac{1}{n} \sum_{b \in \Delta} \boldsymbol{r_b}.$$

The force on vertex a is then given by the gradient of the whole sheet energy $\mathscr{E}_{\text{sheet}}$, which is the sum of the energies $\mathscr{E}_\Delta$ corresponding to each cell Δ.

$$\frac{d\mathscr{E}_{\text{sheet}}}{d\boldsymbol{r_a}} = \frac{d}{d\boldsymbol{r_a}} \sum_\Delta \mathscr{E}_\Delta = \sum_{\Delta : a \in \Delta} \frac{d\mathscr{E}_\Delta}{d\boldsymbol{r_a}} = \sum_{\Delta : a \in \Delta} \frac{d}{d\boldsymbol{r_a}} \sum_{b \in \Delta} (\boldsymbol{r_b} - \boldsymbol{r_\Delta})^2.$$

Since $\boldsymbol{r_\Delta}$ depends on $\boldsymbol{r_a}$ itself, we write

$$
\boldsymbol{f}_{\text{on } a} = -\sum_{\Delta:a\in\Delta} \frac{d}{d\boldsymbol{r_a}} \sum_{b\in\Delta} \left(\boldsymbol{r_b} - \frac{1}{n} \sum_{c\in\Delta} \boldsymbol{r_c} \right)^2
$$

$$
= \sum_{\Delta:a\in\Delta}\sum_{b\in\Delta} \left(2\boldsymbol{r_a}\delta_{ab} - \frac{2}{n}\sum_{c\in\Delta}(\boldsymbol{r_c}\delta_{ab} + \boldsymbol{r_b}\delta_{ac}) + \frac{1}{n^2}\sum_{c\in\Delta}\sum_{d\in\Delta}(\delta_{ac}\boldsymbol{r_d} + \delta_{ad}\boldsymbol{r_c}) \right)
$$

$$
= -2\left(\boldsymbol{r_a} - \boldsymbol{r_\Delta} \right)
$$

This process was overkill, since we could have reasonably assumed that $\boldsymbol{r_\Delta}$ would be at the vertices' center of mass and that we'd effectively get springs from $\boldsymbol{r_\Delta}$ to each vertex. This is thanks to linearity of the collar springs. However, assuming that the collars have a positive equilibrium length r_0 makes it necessary to go through the above procedure.

If instead the line energy is

$$
\mathscr{E}_{ab} = \int_0^1 \left(|\boldsymbol{r_a}t + (1-t)\boldsymbol{r_b} - \boldsymbol{r_\Delta}| - r_0 \right)^2 dt,
$$

then the cell position $\boldsymbol{r_\Delta}$ is the solution to

$$
0 = -2\sum_{b\in\Delta}\boldsymbol{r_b} + 6\boldsymbol{r_\Delta} - 2r_0\frac{d}{d\boldsymbol{r_\Delta}} \sum_{(b,c)\text{ edge in }\Delta} \int_0^1 |\boldsymbol{r_b}t - (1-t)\boldsymbol{r_c} - \boldsymbol{r_\Delta}| \, dt
$$

$$
0 = -2\sum_{b\in\Delta}\boldsymbol{r_b} + 6\boldsymbol{r_\Delta} - 2r_0 \sum_{(b,c)} \int_0^1 \frac{\boldsymbol{r_\Delta} - \boldsymbol{r_c} - t(\boldsymbol{r_b} - \boldsymbol{r_c})}{|\boldsymbol{r_b}t - (1-t)\boldsymbol{r_c} - \boldsymbol{r_\Delta}|} \, dt.
$$

We can actually evaluate the integral above, but I found that it gives a transcendental equation for $\boldsymbol{r_\Delta}$ and decided it wasn't pursuing further on paper. Nonzero equilibrium length springs is better pursued numerically. Alternatively, we simply define springs from $\boldsymbol{r_\Delta}$ to each dual graph vertex rather than making the collars consist of continuous springs.

Bending

One way to define a bending energy is to give each cell a vector that corresponds to the midline pointing out from the center of the cell, which I have implicitly drawn in the figures

of individuals flexas. From there, we could reasonably define a bending energy from the   1
interactions between two interacting flexas by the angle between their corresponding "normal"   2
vectors weighted by the length of their interface.   3

Defining an individual vector is made complicated by the fact that the vertices along the   4
cycles corresponding to each flexa are not necessarily coplanar, provided that a given cell   5
is interacting with more than three other cells. One option, although I have not developed   6
it, is to find the plane whose summed mean squared distances to each vertex for a cell is   7
minimised. It would possibly be more accurate to again treat the edges as lines and minimise   8
the integrated distance from the normal plane to the edges. Either way, the energy dictated   9
by the angle between adjacent normal vectors will need to be summed over all pairs of   10
neighboring cells, namely all edges in the graph where edges correspond to cell neighbors   11
(not collar interfaces).   12

3.6.3   Surface formed by cell bodies   13

The graph of cell bodies and neighbor edges makes it easy to work with springs, but it is less   14
clear how to define a bending energy. The math for springs is identical to previously, so let's   15
just think about how to define bending energy.   16

ak2351: needs more work   17

3.7   Including both cells and collar boundaries   18

3.7.1   Initial sheet   19

3.7.2   Numerical optimisation routine   20

Finally, we numerically optimise. I changed ϕ_0 to be defined relative to the initial value of   21
ϕ, and likewise for ψ. If we make ϕ_0 smaller and ψ_0 larger, we expect the cell collars to   22
contract and for cell-cell distances to lengthen. In other words, we expect the sheet to curve   23
upward, so that the cells on the edges go in the direction that the collars are.   24

The numerical optimisation problem gives a clean sensible solution, which is shown   25
projected onto the *xy*-plane in Figure 3.9. We can tell that the sheet is curved just looking at   26
this alone, which is a massive relief and confirmation of what we expect.   27

The solution in Figure 3.9 is for $\phi_0 = 0.99\phi_{\text{init}}$ and $\phi_0 = 1.03\psi_{\text{init}}$, where ϕ_{init} and ψ_{init} 28
are the initial angles in the flat sheet state. We could now bask in the glory of our solution   29
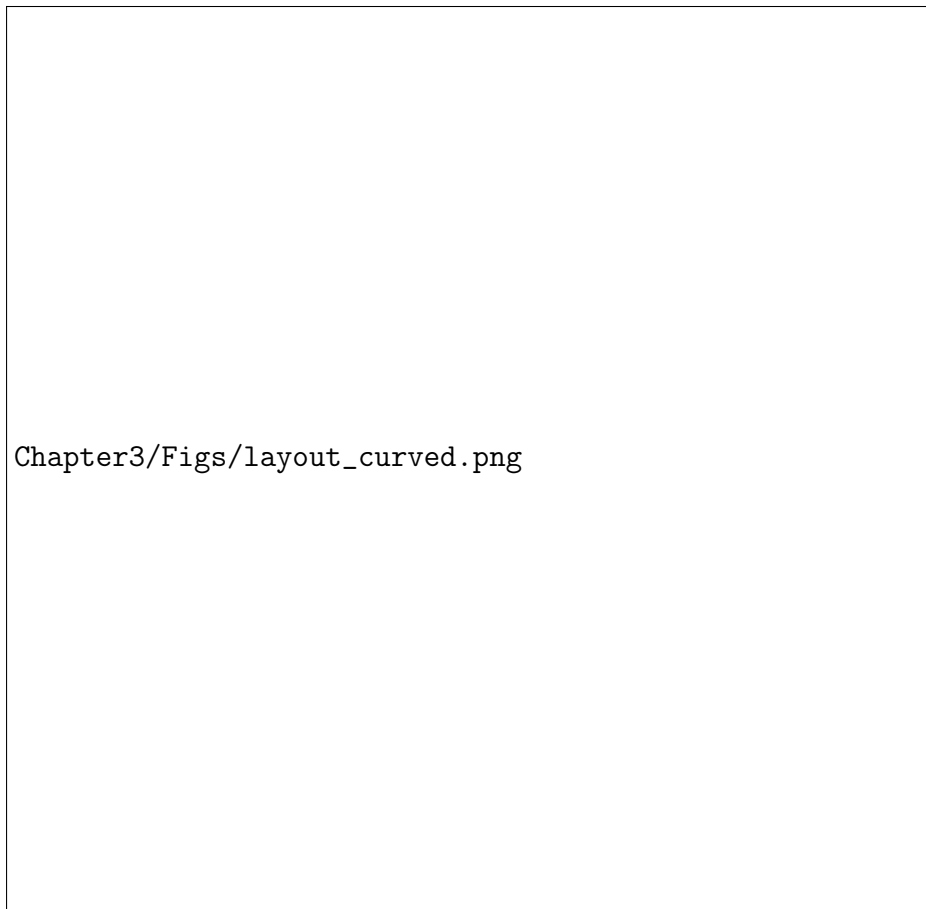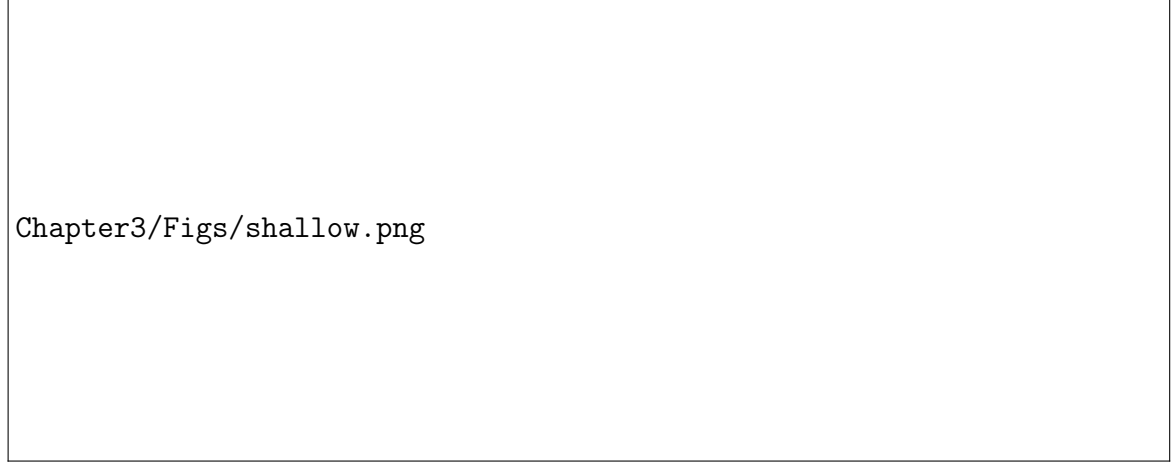and look at it in 3d (Figure 3.10a).   30

Fig. 3.9 Figure in the same style of Figure 3.2 showing the cell sheet projected onto the *xy*-plane after minimising energy.

The resulting structure is really pretty sensitive to small changes in ϕ_0, ψ_0. Figure 3.10b shows the structure that comes out of $\phi_0 = 0.9\phi_{\text{init}}$, $\psi_0 = 1.15\psi_{\text{init}}$.
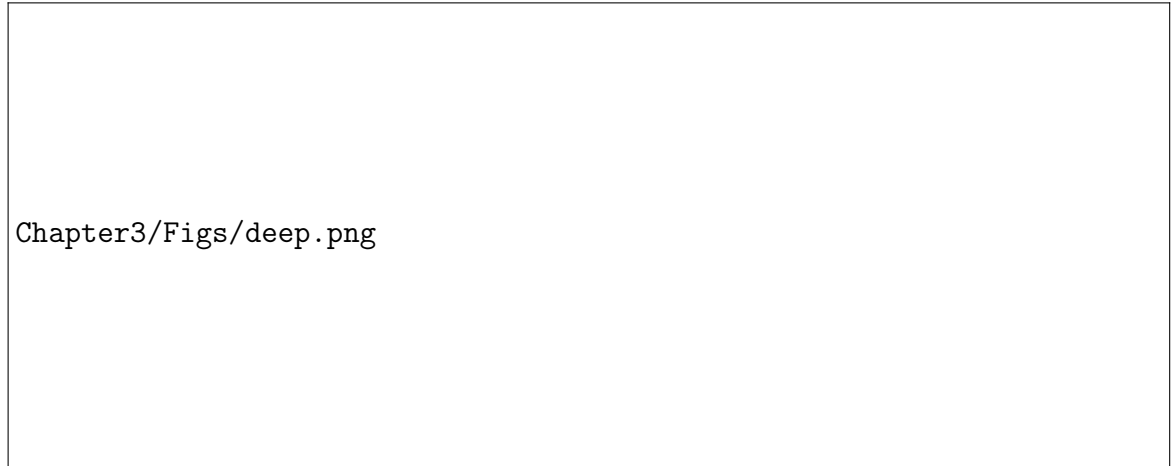

Chapter3/Figs/shallow.png

(a)

Chapter3/Figs/deep.png

(b) 3d projections of the curved sheet formed by $\phi_0 = 0.9\phi_{\text{init}}$, $\psi_0 = 1.15\psi_{\text{init}}$.

Fig. 3.10 Cell sheet geometry from the hexagonal lattice in Figure 3.2 and parameters (3.10a) $\phi_0 = 0.99\phi_{\text{init}}$, $\phi_0 = 1.03\psi_{\text{init}}$, $\ell_0 = \ell_{\text{init}} = 1.52$, (3.10b) $\phi_0 = 0.9\phi_{\text{init}}$, $\psi_0 = 1.15\psi_{\text{init}}$, $\ell_0 = \ell_{\text{init}} = 1.52$.

3.7.3   Topology

In section 3.3, I mentioned that the flat sheet is a stable minimum. But it is here because the lattice is regular. A single pentagon in a hexagonal lattice (like a football (soccer) ball, thanks Lloyd) will make it so no ϕ_0 and ψ_0 will make every cell make the other cells flat.

What I think is interesting about this is the connection between graph topology and surface geometry. I think, in a continuous sense, graph topology affects Gaussian curvature through the energy function.

Adding noise to initial cell positions in Figure 3.2

We expect the initial lattice in Figure 3.2 to produce a sheet with 6-fold symmetry. Since the graph of connections is produced by a Voronoi tessellation, small changes to initial boundary cell positions can change the graph topology for boundary cells.

When adding noise to the initial cell positions, the change in topology at some boundary nodes results in substantial effects felt over the sheet. Figure 3.11 shows the effect of different topology at the boundary.

Interior cell topology

We can also add or merge nodes in a regular lattice (Figure 3.2) to introduce nodes with irregular degree. There are more complex ways of making different graph topologies (like Lloyd's initial icosphere) but I don't have curved initial conditions or more complicated lattices implemented yet.

Figure 3.12 shows a sheet with cell of degree 7 (7 bordering cells) and 3.13 shows a sheet with two neighboring cells of degree 5.

3.7.4   Larger cell sheets

If if inverting a sheet of cells involves flattening it out at the edges, then a small sheet will be able to do this easier than a large one. This is because the cells on the outside have to stretch their collars less if the sheet is smaller when they flatten out.
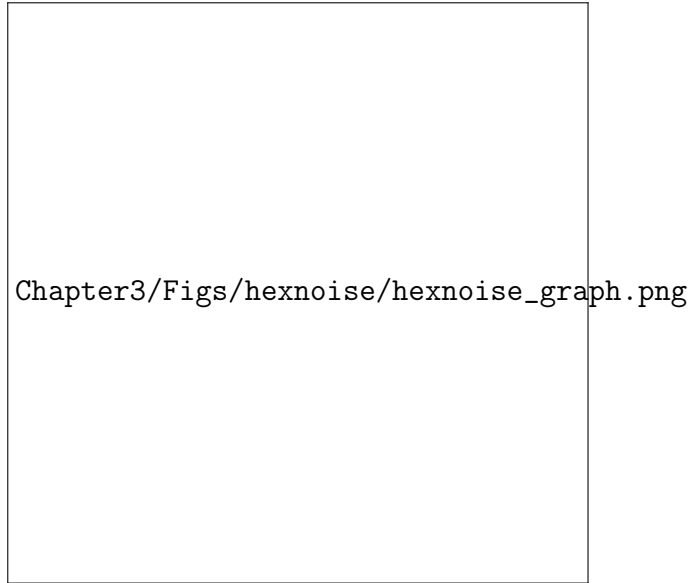
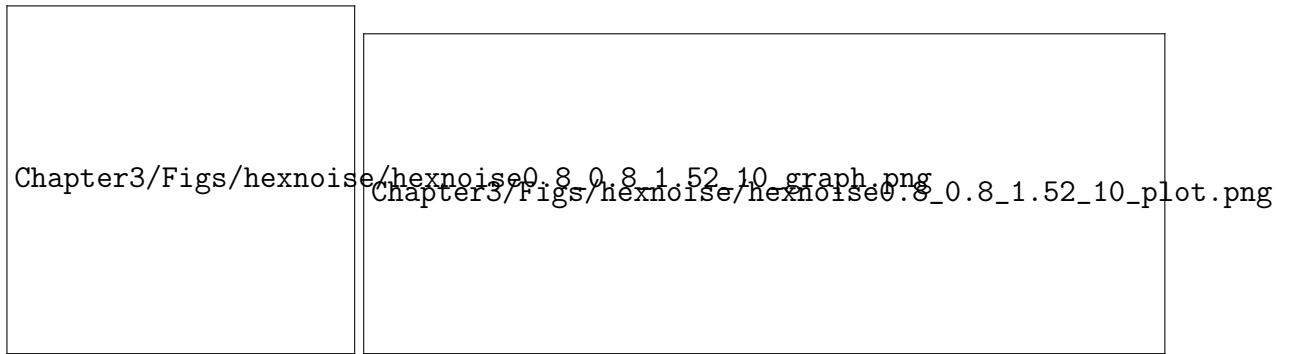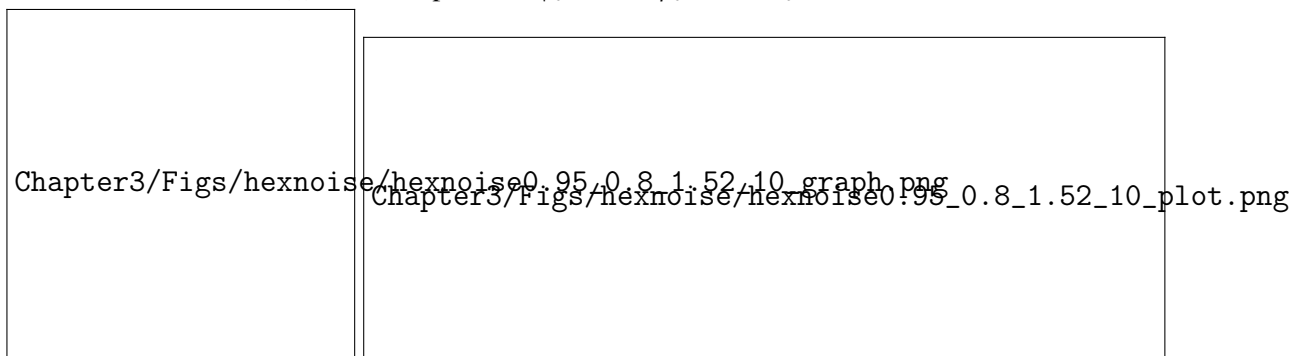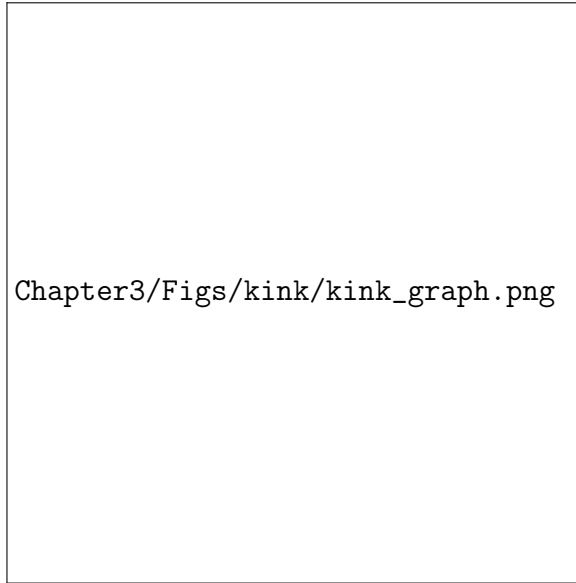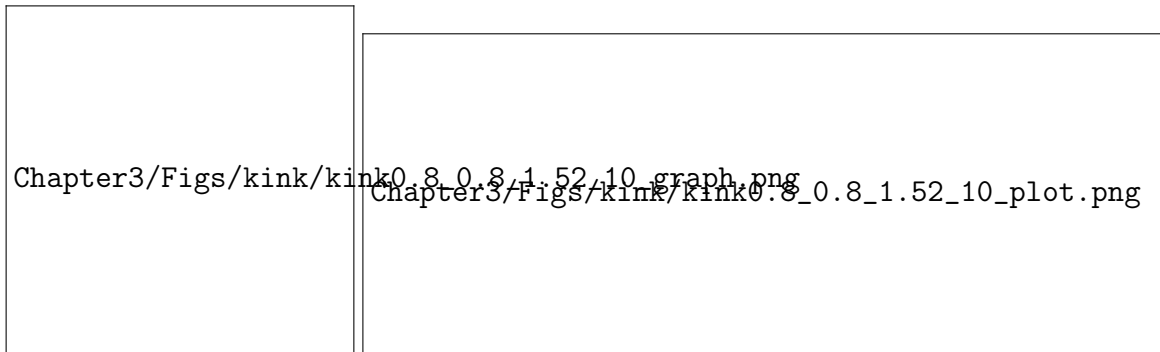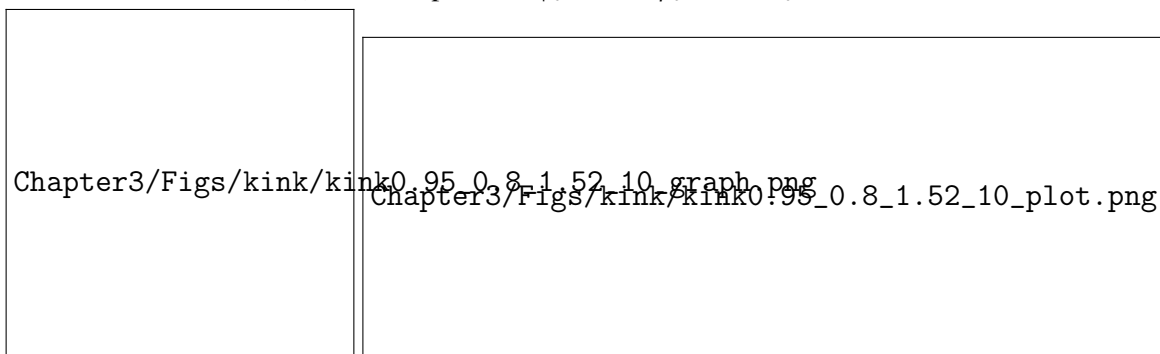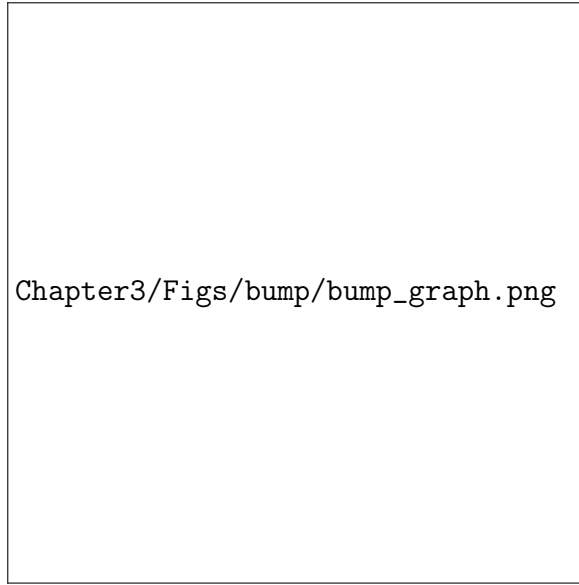(a) Initial lattice drawn as in Figure 3.2.

(b) Sheet shape when $\phi_0 = 0.8$, $\psi_0 = 0.8$, $\ell_0 = 1.52$.

(c) Sheet shape when $\phi_0 = 0.95$, $\psi_0 = 0.8$, $\ell_0 = 1.52$.

Fig. 3.11 Cell sheet geometry with noise added to the initial lattice. The graph topology is affected at the sheet boundary (subfigure 3.11a) from the Voronoi tesselation. This minor change has substantial effects on the sheet geometry (subfigures 3.11b, 3.11c).

(a) Initial lattice drawn as in Figure 3.2.

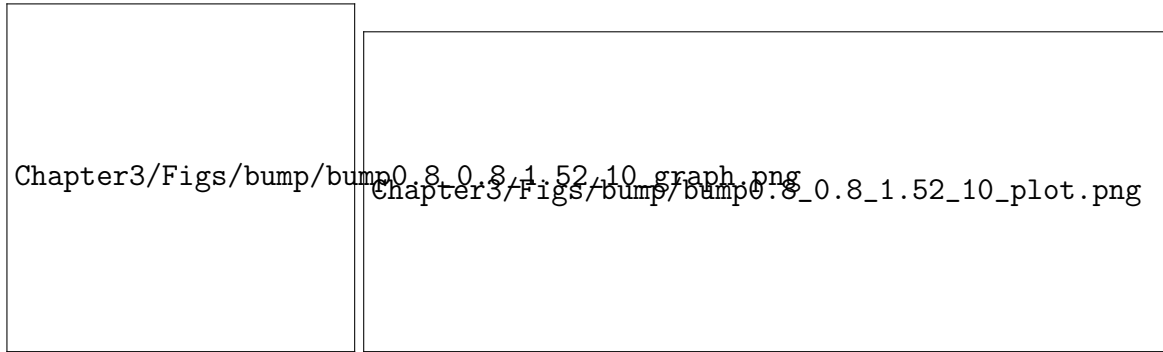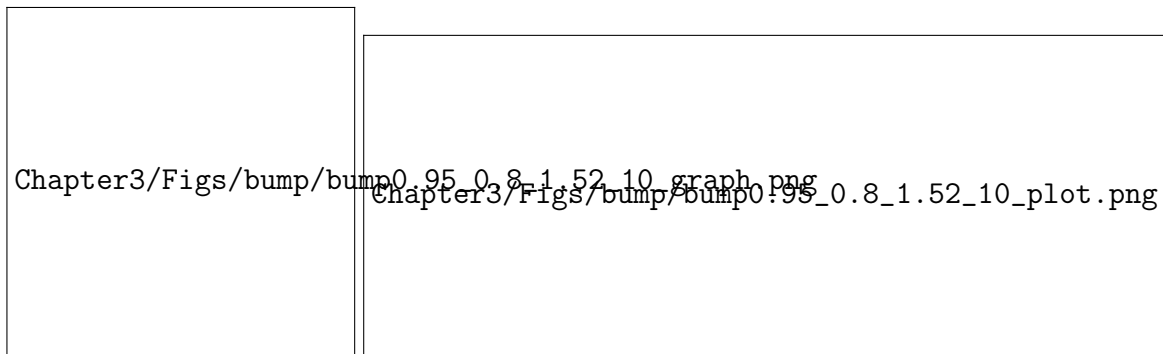

(b) Sheet shape when $\phi_0 = 0.8$, $\psi_0 = 0.8$, $\ell_0 = 1.52$.

(c) Sheet shape when $\phi_0 = 0.95$, $\psi_0 = 0.8$, $\ell_0 = 1.52$.

Fig. 3.12 Cell sheet geometry with a node of degree 7. The graph topology is affected in the sheet interior (subfigure 3.12a). This minor change has substantial effects on the sheet geometry (subfigures 3.12b, 3.12c).

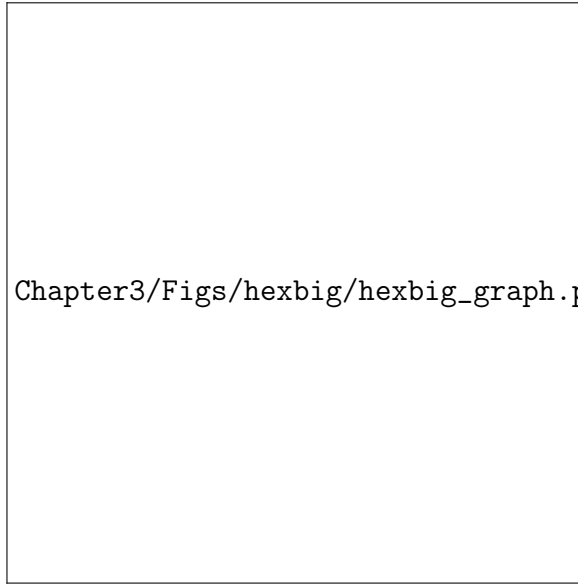(a) Initial lattice drawn as in Figure 3.2.

(b) Sheet shape when $\phi_0 = 0.8$, $\psi_0 = 0.8$, $\ell_0 = 1.52$.

(c) Sheet shape when $\phi_0 = 0.95$, $\psi_0 = 0.8$, $\ell_0 = 1.52$.

Fig. 3.13 Cell sheet geometry with a node of degree 7. The graph topology is affected in the sheet interior (subfigure 3.13a). This minor change has substantial effects on the sheet geometry (subfigures 3.13b, 3.13c).

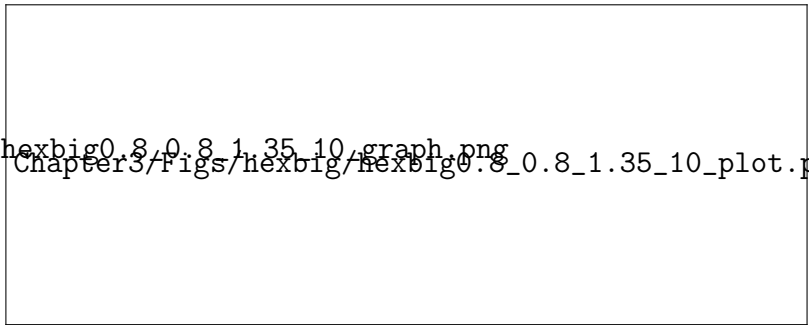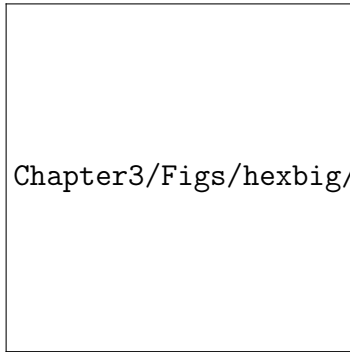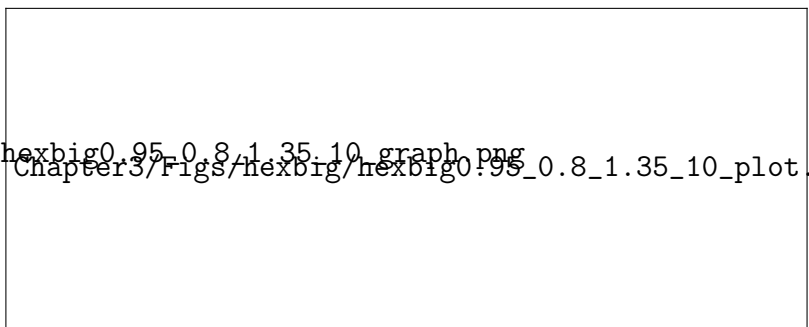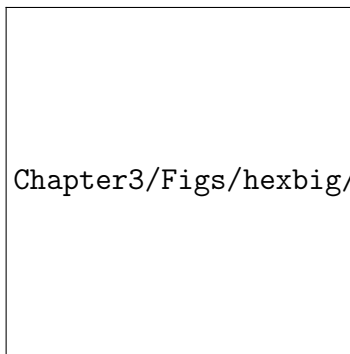(a) Initial lattice drawn as in Figure 3.2.

(b) Sheet shape when $\phi_0 = 0.8$, $\psi_0 = 0.8$, $\ell_0 = 1.52$.

(c) Sheet shape when $\phi_0 = 0.95$, $\psi_0 = 0.8$, $\ell_0 = 1.52$.

Fig. 3.14 Cell sheet geometry with a node of degree 7. The graph topology is affected in the sheet interior (subfigure 3.14a). This minor change has substantial effects on the sheet geometry (subfigures 3.14b, 3.14c).

Chapter 4

Discussion

4.1   section

Think about why *C. flexa* has the behavior that it does. Given how other choanoflagellates like *S. rosetta* get their morphology by division [8, 11], it could be that *C. flexa* forms by division and has evolved its contractile ring to take advantage of that. This would make sense from the perspective that choanoflagellate cells aligned and lined up next to each other drive the strongest flows (though still not stronger than they could individually) Kirkegaard and Goldstein [9]. This paper also found that being farther from a wall increases flux. This is interesting considering that the feeding state of *C. flexa* was observed to be so ineffective at swimming that it sank and remained in place. However this was on a slide and in the absense of external flows Brunet et al. [3].

When thinking about *C. flexa* in the context of multicellularity, we should not overlook the simplicity by which it achieves large-scale geometric changes. While we can develop increasingly complex models by introducing collar filament bending, tension and stress at the collar filaments' bases, or the effects of the contractile ring, my work demonstrates that a coarse description of individual cells is sufficient to explain the behavior that we observe in colonies. Compare this with *Volvox*, which uses connections and communication between cells to control its inversion. One might imagine that the complexity of a molecular pathway for a single cell to exhibit phototaxis or regulate feeding/swimming efficiency could easily exceed the ring contraction as currently understood in *C. flexa* [3].

ak2351: cite Volvox inversion papers, cite papers on phototaxis or swimming signalling pathways

References

[1] Alegado, R. A., Brown, L. W., Cao, S., Dermenjian, R. K., Zuzow, R., Fairclough, S. R., Clardy, J., and King, N. (2012). A bacterial sulfonolipid triggers multicellular development in the closest living relatives of animals. *elife*, 1.

[2] Asadzadeh, S. S., Larsen, P. S., Riisgård, H. U., and Walther, J. H. (2019). Hydrodynamics of the leucon sponge pump. *Journal of the Royal Society Interface*, 16(150):20180630.

[3] Brunet, T., Larson, B. T., Linden, T. A., Vermeij, M. J., McDonald, K., and King, N. (2019). Light-regulated collective contractility in a multicellular choanoflagellate. *Science*, 366(6463):326–334.

[4] Caroli, M., de Castro, P. M., Loriot, S., Rouiller, O., Teillaud, M., and Wormser, C. (2010). Robust and efficient delaunay triangulations of points on or close to a sphere. In *International Symposium on Experimental Algorithms*, pages 462–473. Springer.

[5] Carr, M., Leadbeater, B. S., Hassan, R., Nelson, M., and Baldauf, S. L. (2008). Molecular phylogeny of choanoflagellates, the sister group to metazoa. *Proceedings of the National Academy of Sciences*, 105(43):16641–16646.

[6] Eicke, B. (1992). Iteration methods for convexly constrained ill-posed problems in hilbert space. *Numerical Functional Analysis and Optimization*, 13(5-6):413–429.

[7] Ellis, W. N. (1930). Recent researches on the choanoflagellata (craspedomonadines) (freshwater and marine) with description of new genera and species. *Annales de la Société royale zoologique de Belgique*, 60:49–88.

[8] Fairclough, S. R., Dayel, M. J., and King, N. (2010). Multicellular development in a choanoflagellate. *Current Biology*, 20(20):R875–R876.

[9] Kirkegaard, J. B. and Goldstein, R. E. (2016). Filter-feeding, near-field flows, and the morphologies of colonial choanoflagellates. *Physical Review E*, 94(5):052401.

[10] Landau, L. D., Lifšic, E. M., Lifshitz, E. M., Kosevich, A. M., and Pitaevskii, L. P. (1986). *Theory of elasticity: volume 7*, volume 7. Elsevier.

[11] Larson, B. T., Ruiz-Herrero, T., Lee, S., Kumar, S., Mahadevan, L., and King, N. (2020). Biophysical principles of choanoflagellate self-organization. *Proceedings of the National Academy of Sciences*, 117(3):1303–1311.

[12] Lauterborn, R. (1898). *Protozoën-Studien: IV. T. Flagellaten aus dem Gebiete des Oberrheins. Aus dem Zoologischen Institut der Universität Heidelberg.(M. 2 Taf.)*. A. Lauterborn.

[13] Leadbeater, B. S. (1977). Observations on the life-history and ultrastructure of the marine choanoflagellate choanoeca perplexa ellis. *Journal of the Marine Biological Association of the United Kingdom*, 57(2):285–301.

[14] Leadbeater, B. S. (1983). Life-history and ultrastructure of a new marine species of proterospongia (choanoflagellida). *Journal of the Marine Biological Association of the United Kingdom*, 63(1):135–160.

[15] Leadbeater, B. S. C. (2008). Choanoflagellate evolution: the morphological perspective. *Protistology*, 5:256–267.

[16] Mah, J. L., Christensen-Dalsgaard, K. K., and Leys, S. P. (2014). Choanoflagellate and choanocyte collar-flagellar systems and the assumption of homology. *Evolution & development*, 16(1):25–37.

[17] Michelin, S. and Lauga, E. (2011). Optimal feeding is optimal swimming for all péclet numbers. *Physics of Fluids*, 23(10):101901.

[18] Powers, T. R. (2010). Dynamics of filaments and membranes in a viscous fluid. *Reviews of Modern Physics*, 82(2):1607.

[19] Stokes, G. G. et al. (1851). On the effect of the internal friction of fluids on the motion of pendulums. *Transactions of the Cambridge Philosophical Society*.

[20] Wiggins, C. H., Riveline, D., Ott, A., and Goldstein, R. E. (1998). Trapping and wiggling: elastohydrodynamics of driven microfilaments. *Biophysical journal*, 74(2):1043–1060.